MODERN STUDIES IN

EARTHQUAKE, STRUCTURAL, AND SOIL ENGINEERING

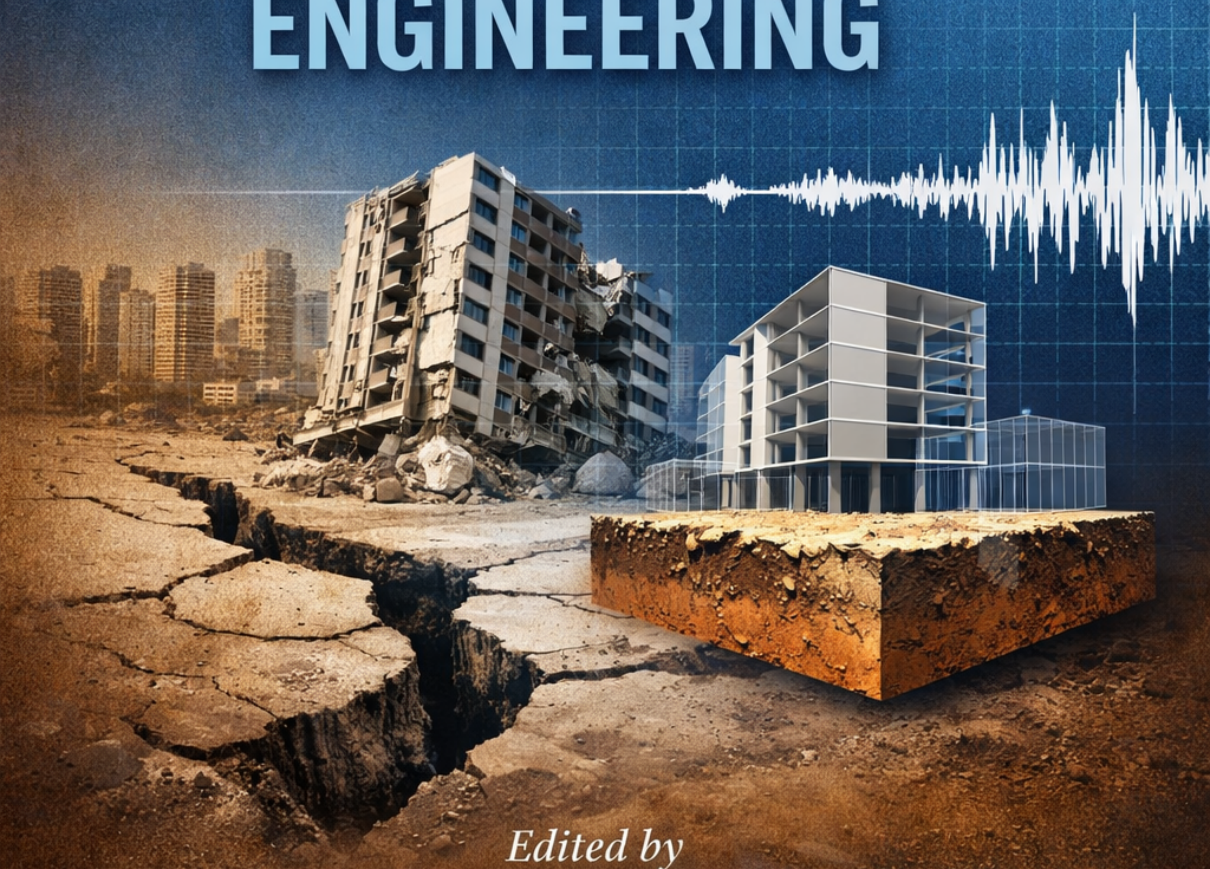

Edited by

Marcos Pérez Mendoza

MODERN STUDIES IN EARTHQUAKE, STRUCTURAL, AND SOIL ENGINEERING- 2026

ISBN: 978-625-93333-4-2

DOI: 10.5281/zenodo.18622523

Edited By

Marcos Pérez Mendoza

February / 2026

İstanbul, Türkiye

Date: 12.02.2026

Halic Publishing House
İstanbul, Türkiye
www.halicyayinevi.com

adopted by Esra KOÇAK
ISBN: 978-625-93333-4-2

MODERN STUDIES IN EARTHQUAKE, STRUCTURAL, AND SOIL ENGINEERING

EDITOR
Marcos Pérez Mendoza

AUTHORS
Mahfoud TOUHARI
Mohammed OUALI
Hanene HAFSI
Naoual HANDEL
S. S. OMOPARIOLA
A. A. ADEALA
Y. KELLOUCHE
H. GADOURI
B. MEZIANI
W. BOUKHLIFA

TABLE OF CONTENTS

PREFACE

This book presents a collection of interdisciplinary studies addressing key challenges in structural engineering, geotechnical innovation, and environmental sustainability. The chapters collectively emphasize performance-based assessment, resilience, and the application of advanced analytical methods in engineering and development contexts.

The first two chapters focus on structural systems and materials, examining the seismic performance of self-supporting structures in accordance with RPA2024 and Eurocode 8, as well as reviewing the critical factors affecting the behavior and performance of concrete-filled steel tube (CFST) structures. These contributions provide important insights for improving safety, reliability, and design efficiency in modern construction.

The third chapter extends the discussion to climate adaptation in the agricultural sector, analyzing the role of irrigation facilities in mitigating the adverse impacts of climate change on agricultural productivity in south-western Nigeria. It highlights the importance of sustainable infrastructure in supporting food security and regional development.

The final chapter introduces a data-driven approach to geotechnical engineering, combining experimental validation with a GA-optimized artificial neural network to predict the behavior of lime-stabilized expansive clay. This innovative methodology demonstrates the growing role of intelligent modeling techniques in advancing material characterization and engineering practice.

Editorial Team
February 12, 2026
Türkiye

CHAPTER 1
STUDY OF THE SEISMIC PERFORMANCE OF SELF-SUPPORTING STRUCTURES ACCORDING TO RPA2024 AND EUROCODE 8: CASE OF THE BEHAVIOR FACTOR

Mahfoud TOUHARI[1]
Mohammed OUALI[2]

[1]Acoustics and Civil Engineering Laboratory Faculty of Sciences and Technology Djilali Bounaama University of Khemis Miliana, Algeria, m.touhari@univ-dbkm.dz, ORCID ID: 0000-0003-3170-0301
[2]Acoustics and Civil Engineering Laboratory, Faculty of Sciences and Technology, Djilali Bounaama University of Khemis Miliana, Algeria, m.ouali@univ-dbkm.dz ORCID ID: 0009-0006-7428-2102

INTRODUCTION

Rapid urban expansion has contributed to the widespread construction of taller reinforced concrete buildings and more flexible structural systems, particularly in seismically active regions. Achieving seismic safety for these structures remains a fundamental challenge, as their seismic response depends heavily on their geometric characteristics and non-linear structural behavior. Although modern seismic design codes provide simplified methodologies for earthquake-resistant design, the accuracy of seismic performance estimation remains closely linked to the analysis methods used and their ability to realistically represent the non-linear behavior of structures. (Federal Emergency Management Agency FEMA, 2000; Fardis, 2005).

Traditional linear elastic analysis methods, commonly used in design practice, have been shown to be inadequate for realistically capturing the behavior of RC structures under strong ground motions, especially when significant damage and plastic deformations occur (Krawinkler, 1996; Fajfar, 2000). To account for inelastic behavior, seismic design relies on the concept of the behavior factor (q or R), which reduces elastic seismic forces by incorporating ductility, over-strength, and energy dissipation capacity. However, the estimation of this factor is highly sensitive to structural geometry and configuration, including building height, bay length, stiffness distribution, and deformation capacity (Lam et al., 1998).

High-rise buildings, in particular, are more prone to a deterioration in rigidity and an increase in lateral deformation. Furthermore, increased spans generally lead to a decrease in lateral rigidity and a reduction in reserve strength, which can adversely affect their seismic performance. To overcome the limitations of linear methods, non-linear impulse analysis is widely used in performance-based seismic design frameworks. This approach allows for the evaluation of overall capacity, tracking of ductility evolution, monitoring of stiffness degradation, and identification of potential failure mechanisms in reinforced concrete frame structures. (Chopra and Goel, 2002). Compared to nonlinear time-history analysis, which requires a large number of ground motion records and significant computational effort, pushover analysis offers a practical and sufficiently accurate alternative for parametric investigations focused on comparative seismic performance.

Despite extensive research on RC frames, the combined influence of building height and bay length on the behavior factor and overall seismic performance remains insufficiently quantified. In this context, the present study aims to investigate the effects of these key geometric parameters on RC frame structures. A series of RC frame models with varying heights (3, 6, 9, and 12 stories) and bay lengths ranging from 3 m to 6 m are analyzed using nonlinear static pushover analysis. The objective is to evaluate global seismic capacity and the main components of the behavior factor, particularly ductility and over-strength, and to clarify geometry-dependent trends that may contribute to improving code-based assumptions and performance.

1. NUMERICAL MODELING AND SEISMIC ANALYSIS PROCEDURE

The seismic performance of reinforced concrete (RC) moment-resisting frames was evaluated using nonlinear static pushover analysis, in accordance with the recommendations of (Federal Emergency Management Agency FEMA, 2000) and (Applied Technology Council ATC, 1996). This method was adopted due to its effectiveness in capturing nonlinear behavior, strength degradation, and energy dissipation capacity of structures subjected to seismic loading.

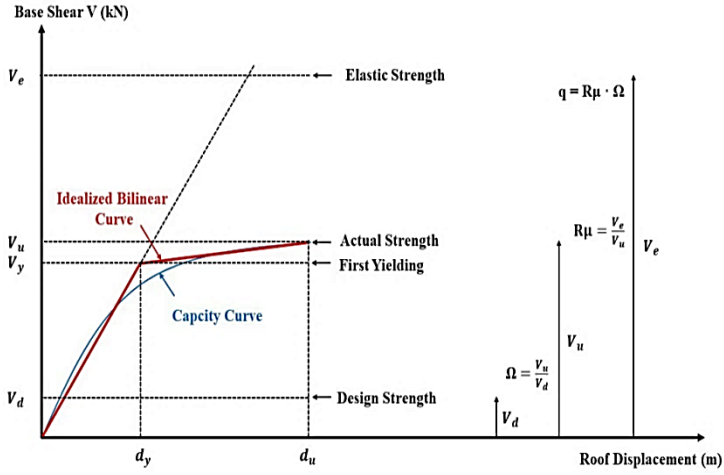

Figure 1. Representative of Capacity Curve (Applied Technology Council ATC, 1996)

A set of reinforced concrete structural models with varying geometric properties was developed to study the effect of building height and opening length on seismic response and to evaluate the behavior coefficient. The effect of building height was examined using four structural models consisting of 3, 6, 9, and 12 stories, designed according to code requirements. (Fardis, 2005). Material properties, section dimensions, and reinforcement details were assigned according to software. Nonlinear static pushover analyses were performed by applying monotonically increasing lateral loads until the formation of global collapse mechanisms. The resulting base shear–roof displacement relationships were recorded to generate capacity curves. These curves were then converted into linear binary representations in accordance with FEMA guidelines (Federal Emergency Management Agency FEMA, 2000), with the aim of enabling the extraction of basic seismic parameters, which include flexible base shear (Ve), maximum base shear (Vu), base shear at yield (Vy), and design base shear (Vd).

2. EVALUATION OF THE BEHAVIOR FACTOR (Q)

The seismic behavior factor (q), which accounts for the inelastic deformation capacity of structures, was evaluated based on the decomposition approach commonly adopted in seismic design codes. The behavior factor was calculated as:

$$q = \frac{V_e}{V_d} = \frac{V_e}{V_u} \cdot \frac{V_u}{V_y} \cdot \frac{V_y}{V_d} = R_\mu . R_\rho . R_\Omega \qquad (2)$$

Where

$$R_\mu = \frac{V_e}{V_u}, \quad R_\rho = \frac{V_u}{V_y}, \quad R_\Omega = \frac{V_y}{V_d}, \qquad (3)$$

Where Rμ represents the ductility factor, Rρ the over-strength factor, and RΩ the redundancy factor. This formulation is consistent with the philosophy of earthquake-resistant design, which allows structures to experience controlled inelastic behavior under severe seismic excitation while remaining safe. In line with the requirements of NEHRP (Federal Emergency Management Agency FEMA, 1994), the response reduction factor expresses the combined effects of ductility, excess resistance, and energy dissipation capacity, allowing elastic seismic forces to be converted into lower design forces.

In this study, redundancy is considered a contributing factor to excess resistance, in line with the practice adopted in US seismic codes (Federal Emergency Management Agency FEMA, 2000), rather than an independent factor as stated in ATC (Applied Technology Council ATC, 1995). This unified approach contributes to a consistent and systematic evaluation of the influence of building height and geometry on seismic behavior and the estimation of behavior factors, providing a reliable framework for seismic comparisons.

2.1 Structural Models and Design

A comprehensive numerical investigation was conducted on reinforced concrete (RC) moment-resisting frame structures to examine the influence of both building height and bay length on seismic performance. Two sets of models were considered:

- **Height variation models:** Four RC frames with 3, 6, 9, and 12 stories were analyzed to study the impact of height on global seismic response and the behavior factor (q).

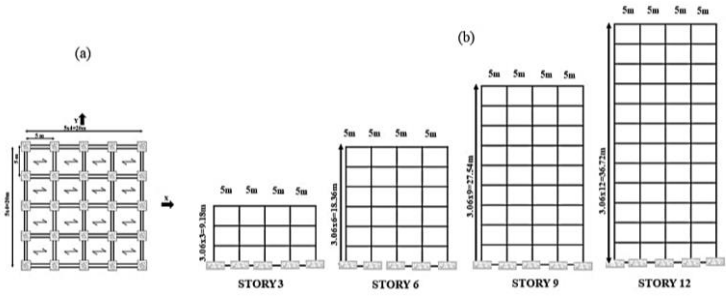

Figure 2. (a) Plan Views (b) Different Story-Structures

- **Bay length variation models:** Four six-story frames with bay lengths of 3, 4, 5, and 6 meters were examined to assess the effect of span length on lateral stiffness, ductility, over-strength, and behavior factor.

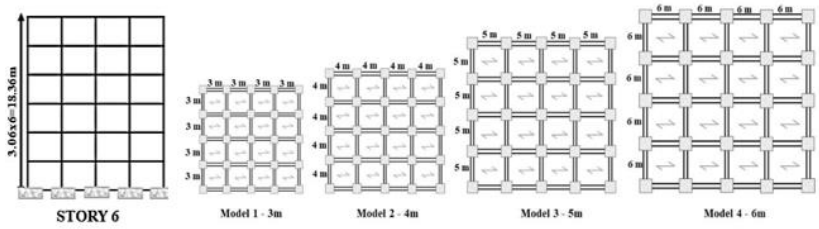

Figure 3. Plan Views of Structures Studied

All models were designed according to Eurocode 8 (Fardis, 2005) and the Algerian seismic code RPA 2024 Ministry of Housing, Urbanism and the City. (2024) for RC design and seismic loading. Concrete of class C25/30 and reinforcing steel of grade B450 (fy = 420 MPa, Ec = 25,000 MPa, Poisson's ratio = 0.30) were used. Column and beam cross-sectional dimensions and reinforcement details are provided in Tables 2 and 3. Floor heights were uniform at 3.06 m, resulting in total heights of 9.18 m to 36.72 m for height variation models, and 18.36 m for bay variation models.

Numerical Modeling Approach

All structures were modeled in ETABS 2021 as 2D RC moment-resisting frames with fixed bases, neglecting soil–structure interaction. Nonlinear behavior was simulated using a lumped plasticity approach, with nonlinear flexural hinges assigned at beam and column ends in accordance with FEMA 356 (Federal Emergency Management Agency FEMA, 2000) and ATC-40(Applied Technology Council ATC, 1996) guidelines. Hinge properties followed moment–rotation relationships corresponding to performance levels: Immediate Occupancy (IO), Life Safety (LS), and Collapse Prevention (CP). Geometric nonlinearity (P–Δ effects) and Rayleigh damping of 5% were included.

Table 1. Design Data for Dynamic Parameters

Sl.no	Seismic Zone	III
1	Zone acceleration coefficient	0,25
2	Damping correction factor	0,875
3	Average dynamic amplification factor	2.338
4	Behavior factor q	5.5
5	Soil type	Medium soil (S3)
6	Frame type	Special Moment Resisting Frame

Table 2. Column Dimensions and Reinforcement Details

Story / ***Structure***	***Cross section- Steel bars***	***1 and 2***	***3 and 4***	***5 and 6***	***7 and 8***	***9 and 10***	***11 and 12***
3 St	cross section	**50 x 50 cm²**	**45 x 45 cm²**				
	steel bars	4T16+12T14	16T14				
6 St	cross section	**65 x 65 cm²**	**60 x 60 cm²**	**55 x 55 cm²**			
	steel bars	16T20	4T20+12T16	16T16			
9 St	cross section	**80 x 80 cm²**	**75 x 75 cm²**	**70 x 70 cm²**	**65 x 65 cm²**	**60 x 60 cm²**	
	steel bars	4T25+16T20	20T20	16T20	16T20	4T20+12T16	
12 St	cross section	**95 x 95 cm²**	**90 x 90 cm²**	**85 x 85 cm²**	**80 x 80 cm²**	**75 x 75 cm²**	**70 x 70 cm²**
	steel bars	4T32+20T20	4T25+20T20	24T20	4T25+16T20	20T20	16T20

Table 3. Beam Dimensions and Reinforcement Details

Story / ***Structure***	***Cross section- Steel bars***	***1 and 2***	***3 and 4***	***5 and 6***	***7 and 8***	***9 and 10***	***11 and 12***
3 St	cross section (cm^2)	35*30	35*30				
	steel in span	6.8	6.8				
	steel on support	4.5	4.5				
6 St	cross section (cm^2)	35*50	35*50	35*50			
	steel in span	9.4	9.4	9.4			
	steel on support	8.4	8.4	8.4			
9 St	cross section (cm^2)	40*50	40*50	40*50	40*50	40*50	
	steel in span	11.6	11.6	11.6	11.6	11.6	
	steel on support	10.6	10.6	10.6	10.6	10.6	
12 St	cross section (cm^2)	40*60	40*60	40*60	40*60	40*60	40*60
	steel in span	14.6	14.6	14.6	14.6	14.6	14.6
	steel on support	13.6	13.6	13.6	13.6	13.6	13.6

The structures were discretized with an average element length of 0.5 m. Nonlinear static pushover analyses were performed under displacement-controlled loading, following the first mode shape, until significant strength degradation or target displacements were reached. Maximum interstory drift ratios were limited to 3% in accordance with RPA 2024 (Ministry of Housing, Urbanism and the City, 2024) and EC8 (Fardis, 2005).

3. EVALUATION OF SEISMIC BEHAVIOR FACTOR

The behavior factor (q) was computed based on its components: ductility reduction factor (Rμ) and over-strength factor (RΩ)**,** the computed q-values were compared with code recommendations (5.5 in RPA 2024 (Ministry of Housing, Urbanism and the City, 2024), 5.85 in Eurocode 8 (Fardis, 2005). This modeling framework allows a systematic assessment of how both building height and bay length influence the seismic performance and energy dissipation capacity of RC frame structures.

3.1 Results and Discussions

Height Variation Models

The nonlinear pushover analysis was conducted on all models, providing valuable insights into their seismic behavior and performance evaluation.

Capacity Curves: The capacity curves show that the base shear increases with building height, reaching a maximum of about 10,000 kN for the 12-story frame Figure 4. This trend suggests that taller structures develop higher lateral strength due to larger mass and cumulative stiffness, consistent with findings by Fajfar (Fajfar, 2000). However, the increase in displacement demand highlights reduced ductility in higher stories, in line with Chopra (Chopra and Goel, 2002). Such results confirm that structural height significantly influences seismic performance, agreeing with previous pushover analyses.

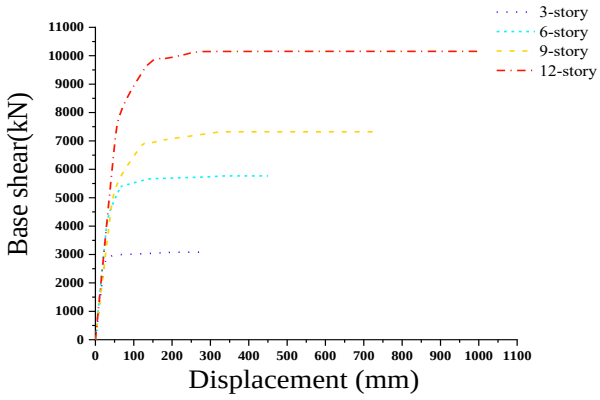

Figure 4. Capacity Curves

Performance Point: The performance points obtained from FEMA 440 (Federal Emergency Management Agency FEMA, 2000) show that shorter buildings (3- and 6-story) reach their demand intersections at lower displacements, while taller frames (9- and 12-story) exhibit higher displacement capacities before failure Figure 5.

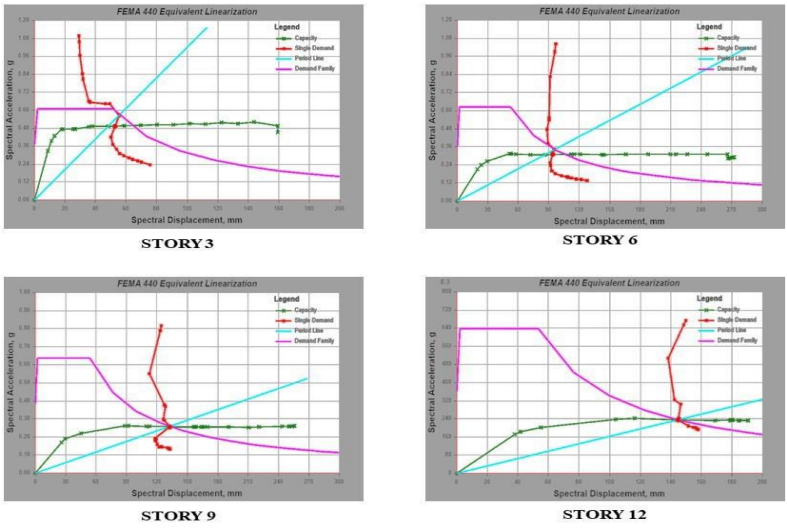

Figure 5. Performance Evaluation Point

This indicates that increasing height improves deformability but reduces energy dissipation efficiency. (Freeman, 1998) Highlighted similar results, confirming the reliability of amplitude-spectrum methods in performance-based design, and (Chopra and Goel, 2002) demonstrated the transformation of performance points with respect to height. These findings support the necessity of height-related performance evaluation in seismic assessment.

Plastics Hinges: Figure 6 illustrates the development and distribution of plastic hinges and deformations as a function of building height and number of stores, where we observe limited deformations and orderly structural behavior for relatively low buildings, indicating better resistance to lateral loads and increased stiffness. In contrast, as the height increases to 9 and 12 stores, lateral deformations and plastic hinge formation become more pronounced, especially in vertical elements, reflecting an escalation in non-linear response. This gradient highlights the transition from quasi-elastic behavior in the lower levels to more elastic behavior in the upper levels, emphasizing the importance of balanced control of stiffness and elasticity distribution along the height to avoid undesirable collapse mechanisms.

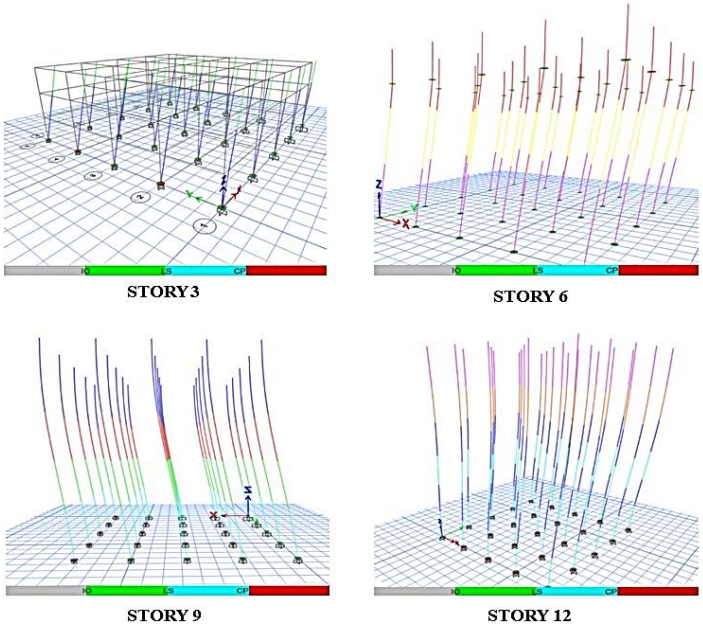

Figure 6. Appearance Of Different Types of Plastic Hinges in Structural Elements

Ductility Factor, Rμ: With changes in the height of the building, the plasticity factor exhibits irregular behavior, as illustrated in Figure 7. The 6-storey structure has the highest ductility value (≈4.1), reflecting an improvement in deformation capacity and energy dissipation. In contrast, the 3-storey building exhibits relatively limited ductility (≈2.7), which is consistent with the brittle behavior typically associated with low-rise buildings according to ATC-40 recommendations (Applied Technology Council ATC, 1996). Taller buildings (9-12 storeys) show a slight decrease in ductility (3.4-3.7), which is attributed to the effect of higher vibration modes and redistribution of soft connections, as reported in FEMA 356 (Federal Emergency Management Agency FEMA, 2000). These results confirm that mid-rise buildings often achieve optimal performance in terms of ductility, which is consistent with the findings of Fajvar (Fajfar, 2000) and Prestley (Lam et al., 1998).

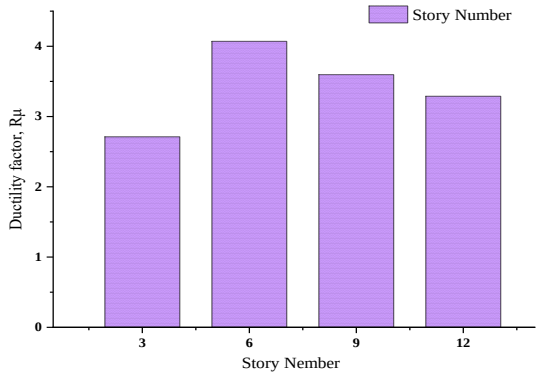

Figure 7. Ductility Factor Histogram

Over strength factor RΩ: The over strength factor (RΩ) exhibits its maximum value in the 3-story frame (≈2.4), highlighting the conservative design capacity of low-rise structures Figure 8.

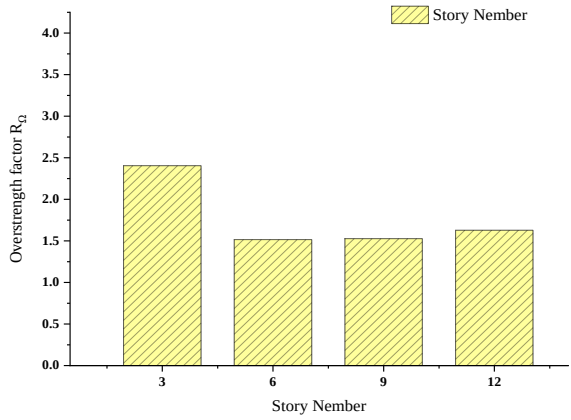

Figure 8. Over Strength Factor RΩ

For high-rise buildings (6 to 12 stories), the excess resistivity coefficient RΩ is relatively constant in the range of 1.5–1.6, indicating a smaller difference between design forces and maximum capacity. This behavior is consistent with the concept that high-rise buildings redistribute seismic demand more evenly, thus limiting the amount of available reserve capacity (Applied Technology Council ATC, 1996).

Similar trends of decreasing excess resistance with increasing height have been reported in FEMA-440 (Federal Emergency Management Agency FEMA, 2000) and Eurocode 8 (Fardis, 2005) studies, confirming that low-rise buildings often have greater excess resistance compared to medium- and high-rise buildings.

Redundancy Factor Rρ: With varying building heights, the repetition factor (Rρ) remains constant and relative, ranging from 1.1 to 1.17, as shown in Figure 9, regardless of the building height, as this uniformity reflects the stability of the number of alternative load transfer paths and the overall distribution of seismic demand. The 9-storey structure has the highest approximate value (≈1.17), indicating a slight improvement in the level of structural redundancy, but this difference remains limited. Similar results were reported in the ATC-19 (Applied Technology Council ATC, 1995) and FEMA P-695 (Federal Emergency Management Agency FEMA, 2009) studies, which found that the contribution of redundancy to reducing seismic demand is less than that of ductility and excess strength. Therefore, Rρ plays a secondary role in defining the overall seismic behavior factor.

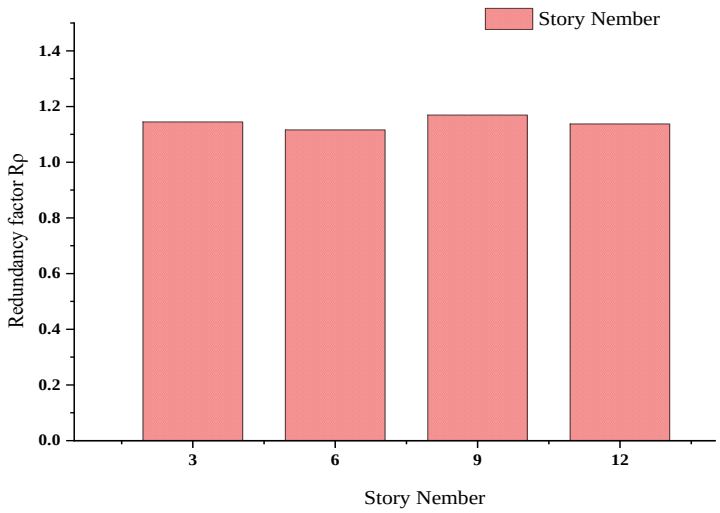

Figure 9. Redundancy factor R_ρ

Behavior factor:

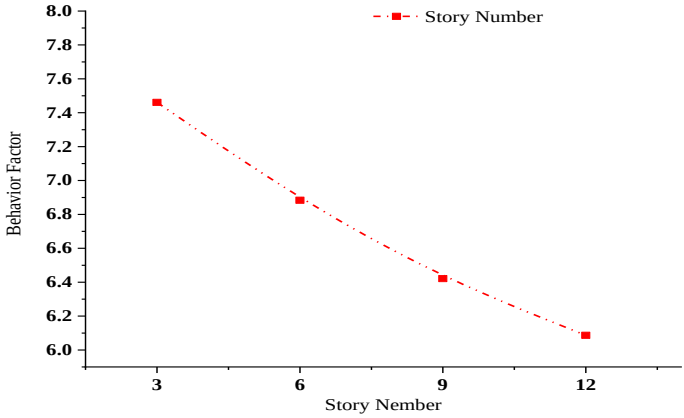

Figure 10. Behavior Factor q

Figure 10 shows a decrease in the structural behavior factor with increasing floor height, with its value decreasing from 7.5 for three-storey structures to around 6. 1 for twelve-storey structures, reflecting the reduced energy dissipation capacity and flexibility of high-rise structures, which negatively affects their seismic resistance. (Miranda & Bertero, 1994), made similar observations, highlighting the effect of height on deformability, a finding corroborated by Krawinkler (Krawinkler, 1996), who supported these results by emphasizing the relationship between the behavior coefficient q and the building's homogeneity and height. These data underscore the necessity of considering the effect of height in the design requirements for earthquake-resistant foundations.

Bay Length Variation Models: The analysis revealed that increasing bay length from 3 m to 6 m raises displacement and drift, reducing stiffness and seismic resistance; thus, longer-span RC frames require enhanced design for stability and deformation control.

Capacity Curves: Table 4 shows that increasing bay length raises base displacement and total ductility while reducing lateral stiffness. Figures 11, 12, and 5 show a wider gap between yield and final displacement, reflecting higher ductility demand and a slight reduction in base shear, consistent with (Meda et al., 2024).

.

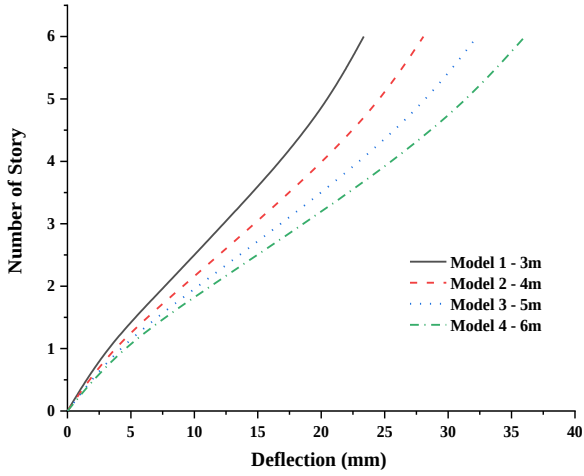

Figure 11. Deflection Depending on The Number of Stories

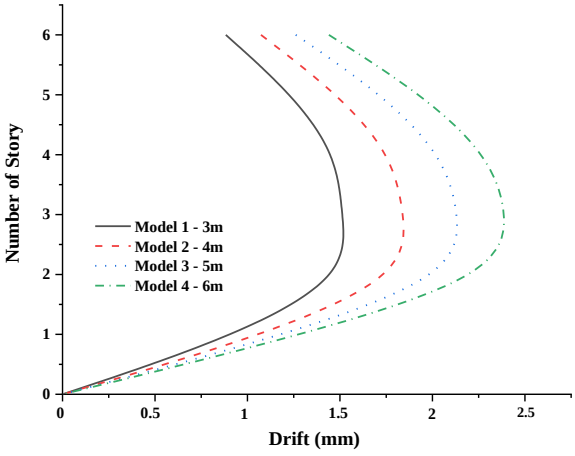

Figure 12. Drift Depending on The Number of Stories

Shorter beams (3 m) provide higher strength, while longer beams (6 m) improve ductility and energy dissipation but lower stiffness and force resistance.

Table 4. Calculation for Components of Factor Q

Model	yield base shear (kN)	Design base shear (kN)	Max Displacement (mm)	yield Displacement (mm)
Model 1	3669.1	1157.5	94.1	39.1
Model 2	3624.9	1733.5	144.3	45.1
Model 3	3558.6	2443.1	174.6	51.0
Model 4	3513.9	3286.4	197.8	57.0

Figure 13 specifically illustrates the variation of roof displacement with base shear for all models, highlighting the effect of bay length on seismic performance. Nonlinear time history analysis is recommended for more accurate evaluation, in line with (Jough & Babaei, 2025).

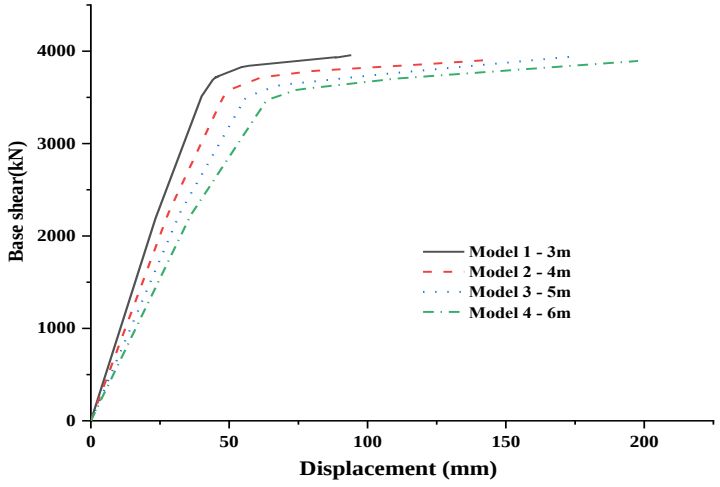

Figure 13. Capacity Curves

Seismic Performance Point: Based on FEMA 440 (Federal Emergency Management Agency FEMA, 2000), results show that increasing beam length shifts performance points toward higher displacements, indicating reduced stiffness figure 14, lower energy dissipation, and greater deformation susceptibility; shorter bays exhibit stronger, more stable seismic behavior, consistent with (Huang et al., 2021).

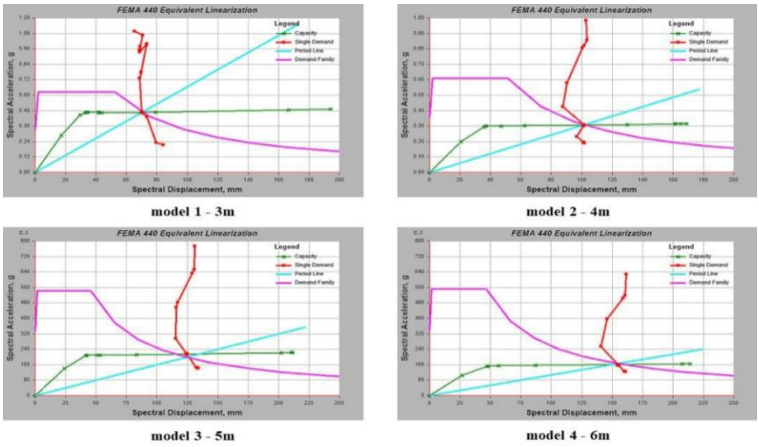

Figure 14. Performance Evaluation Point

Plastics Hinges: Figure 16 illustrates that increasing bay length alters plastic hinge distribution; shorter bays (model 1) show concentrated upper-story deformation and high stiffness, while wider bays (models 3–4) exhibit lower-story hinging, higher ductility, and potential soft-story behavior.

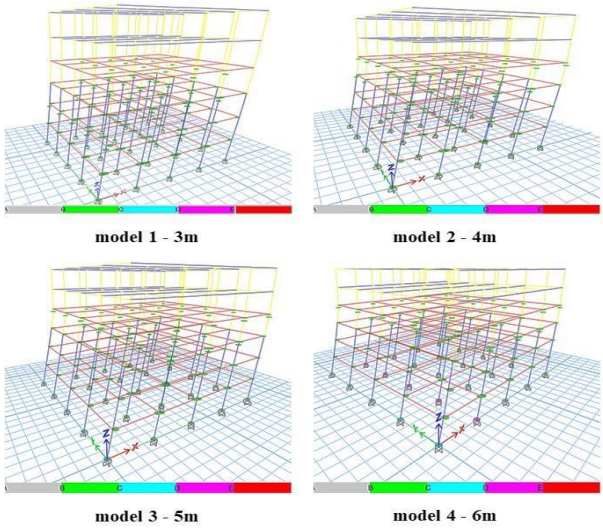

Figure. 16. Appearance Of Different Types of Plastic Hinges in Structural Elements

Ductility factor, Rμ: Ductility reflects a structure's capacity to deform without collapse under seismic loads.

The ductility reduction factor (Rμ), calculated using Newmark and Hall's method, relates elastic and yield strengths, depending on ductility and structural period behavior.

$$\begin{cases} R_u = 1 & \text{for} \quad T < 0.2\ s \\ R_u = \sqrt{(2u-1)} & \text{for} \quad 0.2\ s < T < 0.5\ s \\ R_u = u & \text{for} \quad T > 0.5\ s \end{cases}$$

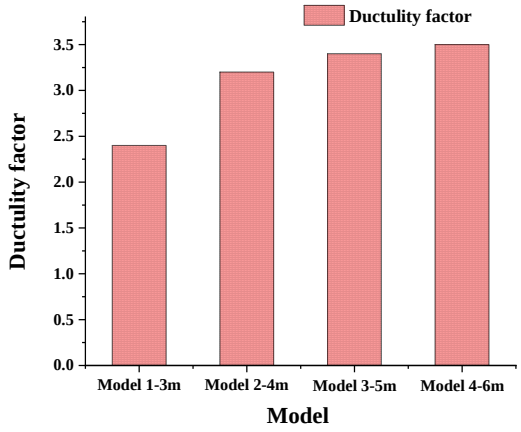

Figure 17. Ductility Reduction Factor (Rμ)

Figure 17 shows that increasing bay length significantly affects ductility; shorter bays exhibit higher ductility factors and elastic behavior, while longer bays, especially model 4, display greater elasto-plastic deformation capacity.

Over Strength Factor RΩ: Figure 18 shows that increasing beam length reduces over strengths, order bays exhibit higher reserve capacity and stiffness concentration, while longer bays show balanced demand distribution but lower seismic resistance, emphasizing bay length's critical role in structural integrity.

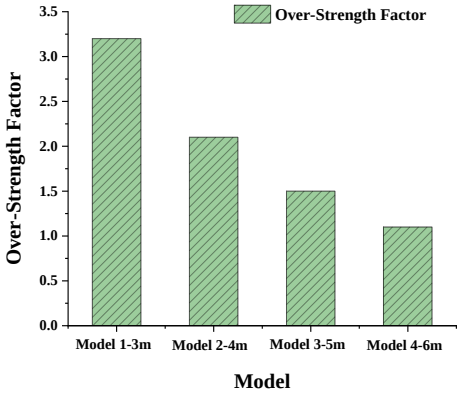

Figure 18. Over-Strength Factor (RΩ)

Redundancy Factor Rρ: The redundancy factor (Rρ) remains nearly constant across the different beam span lengths of the four structural configurations, with values ranging approximately between 1.10 and 1.17 (Figure 19). This stability indicates that variations in beam span length have a negligible effect on load path redundancy and seismic demand distribution. Consistent with ATC-19 (Applied Technology Council ATC, 1995) and FEMA P-695 (Federal Emergency Management Agency FEMA, 2009), the contribution of redundancy is minor compared to ductility and over strength, making Rρ a secondary parameter in defining the overall seismic behavior factor.

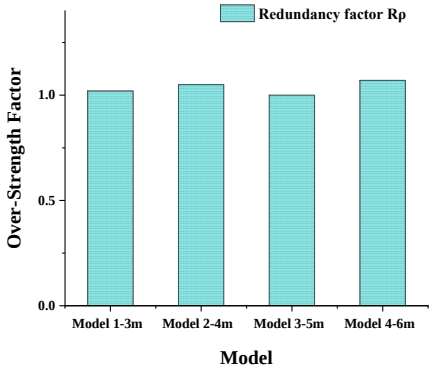

Figure19. Redundancy Factor R_ρ

Behavior Factor (q- factor): Below is a more precise, article-ready paragraph that includes the comparison with RPA2024 (Ministry of Housing, Urbanism and the City, 2024) and Eurocode 8 (Fardis, 2005) and explains the reasons and implications: The results (q = 7.65 for 3 m bays down to q = 3.95 for 6 m bays) demonstrate a clear decline of the seismic behavior factor as bay length increases Figure 20. This trend stems from simultaneous reductions in over-strength (RΩ) and effective ductility (Rμ) when bays widen: shorter bays concentrate stiffness and reserve strength, yielding higher RΩ and a balanced ductile response, whereas longer bays distribute demand, lower stiffness and reserve capacity, and shift deformation toward elasto-plastic mechanisms. Consequently, the computed q-values span both above and below the code recommendations (RPA2024: q = 5.5 (Ministry of Housing, Urbanism and the City, 2024); Eurocode 8: q = 5.85 (Fardis, 2005), indicating that a single, fixed q can be non-representative for differing bay configurations. For reliable design, q should be calibrated to plan geometry (bay length) using nonlinear assessment (pushover or time-history) and detailed Rμ–RΩ evaluation; further validation by nonlinear time-history analyses is recommended.

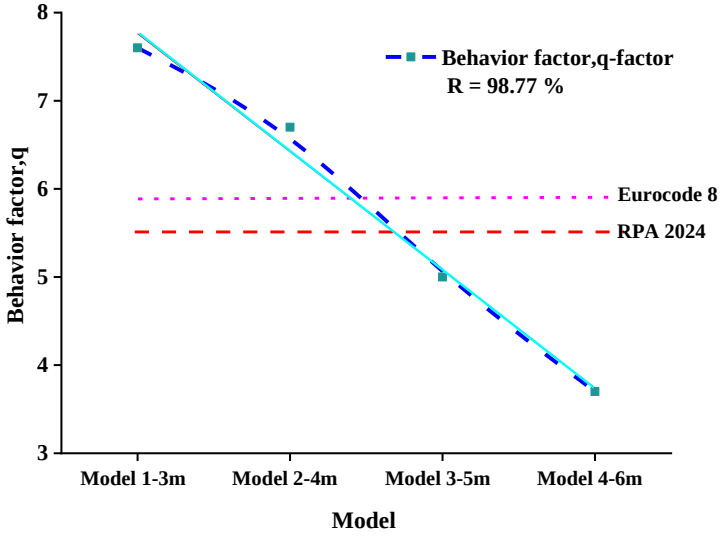

Figure 20. Behavior Coefficient Curve

CONCLUSION

- The seismic performance of reinforced concrete (RC) frames is strongly influenced by building height and bay length.
- Behavior factor (q) decreases with increasing height and larger bay lengths, reflecting reduced energy dissipation capacity.
- Ductility (Rμ / Ru) tends to decrease with taller frames but increases with longer spans, indicating higher deformation capacity in large bay structures.
- Over-strength (RΩ / Rs) decreases with both height and bay length, lowering the safety margin against unexpected seismic loads.
- Stiffness degradation and maximum interstory drift increase with building height, highlighting the need for height-dependent design considerations.
- Shorter, smaller-span buildings provide better seismic performance, with higher behavior factors, greater over-strength, and improved energy dissipation.
- Taller and larger-span frames require careful reinforcement detailing to maintain over-strength and ensure structural safety under seismic excitation.
- These findings emphasize the importance of considering geometric parameters in performance-based seismic design and refining current seismic code provisions.

REFERENCES

Applied Technology Council. (1995). *Structural response modification factors* (ATC-19). ATC.

Applied Technology Council. (1996). *Seismic evaluation and retrofit of concrete buildings* (ATC-40). ATC.

Chopra, A. K., & Goel, R. K. (2002). A modal pushover analysis procedure for estimating seismic demands for buildings. *Earthquake Engineering & Structural Dynamics, 31*(3), 561–582. https://doi.org/10.1002/eqe.144

Da Silva, A., Tsiavos, A., & Stojadinović, B. (2023). Ductility–strength and strength–ductility relations for a constant yield displacement seismic design procedure. *Bulletin of Earthquake Engineering, 21*, 4449–4479. https://doi.org/10.1007/s10518-023-01683-1

Fajfar, P. (2000). A nonlinear analysis method for performance-based seismic design. *Earthquake Spectra, 16*(3), 573–592. https://doi.org/10.1193/1.1586128

Fardis, M. N. (2005). *Designer's guide to EN 1998-1 and EN 1998-5 Eurocode 8: Design of structures for earthquake resistance—General rules, seismic actions, design rules for buildings, foundations and retaining structures*. Thomas Telford.

Federal Emergency Management Agency. (1994). *NEHRP recommended provisions for seismic regulations for new buildings* (FEMA 222A). FEMA.

Federal Emergency Management Agency. (2000). *Prestandard and commentary for the seismic rehabilitation of buildings* (FEMA 356). FEMA.

Federal Emergency Management Agency. (2009). *Quantification of building seismic performance factors* (FEMA P695). FEMA.

Freeman, S. A. (1998). The capacity spectrum method as a tool for seismic design. In *Proceedings of the 11th European Conference on Earthquake Engineering*.

Huang, H., Yuan, Y., Zhang, W., & Li, M. (2021). Seismic behavior of a replaceable artificial controllable plastic hinge for precast concrete beam–column joint. *Engineering Structures, 245*, 112848. https://doi.org/10.1016/j.engstruct.2021.112848

Jough, F., & Babaei, S. (2025). Seismic performance evaluation of space-frame structures using nonlinear static and time-history analyses. *Ömer Halisdemir Üniversitesi Mühendislik Bilimleri Dergisi*. https://doi.org/10.28948/ngumuh.1633034

Krawinkler, H. (1996). Pushover analysis: Why, how, when, and when not to use it. In *Proceedings of the 65th SEAOC Convention* (pp. 91–109).

Lam, N., Wilson, J., & Hutchinson, G. (1998). The ductility reduction factor in the seismic design of buildings. *Earthquake Engineering and Structural Dynamics, 27*, 749–769. https://doi.org/10.1002/(SICI)1096-9845(199807)27:7<749:AID-EQE752>3.0.CO;2-X

Meda, G., Mehta, N., Patel, J., & Butala, A. (2024). Performance-based seismic design of reinforced concrete building. *International Research Journal on Advanced Engineering and Management*. https://doi.org/10.47392/irjaem.2024.0369

Ministry of Housing, Urbanism and the City. (2024). *Algerian seismic design code (RPA 2024): Design and calculation rules for earthquake-resistant structures* (Version 4.0). Algiers, Algeria.

Miranda, E., & Bertero, V. V. (1994). Evaluation of strength reduction factors for earthquake-resistant design. *Earthquake Spectra, 10*(2), 357–379. https://doi.org/10.1193/1.1585778

CHAPTER 2
A REVIEW OF THE FACTORS IMPACTING THE PERFORMANCE OF CFST

Hanene HAFSI[1]
Naoual HANDEL[2]

[1]Department of Civil Engineering, Faculty of Science and Technology INFRARES Laboratory University of Mouhamed Cherif Messadia Souk-Ahras, Algeria, h.hafsi@univ-soukahras.d, ORCID ID: 0009-0008-7917-3495
[2]Department of Civil Engineering, Faculty of Science and Technology INFRARES Laboratory University of Mouhamed Cherif Messadia Souk-Ahras, Algeria, n.handel@univ-soukahras.dz, ORCID ID: 0000-0002-5711-9999.

INTRODUCTION

In recent years, composite columns, such as concrete-filled steel tubes (CFST), have been adopted in many buildings owing to their ability to carry high loads, resistance to buckling, and small cross sections. The high performance of CFST columns is due to the interaction between steel and concrete, known as 'composite action'. This type of column can offer high axial compressive strength even without primary reinforcement or embedded anchoring devices, enabling it to withstand external loads with a reduced cross-section (Ahmed et al., 2019). Furthermore, concrete-filled steel tubular structures (CFSTs) are increasingly used in technical applications in earthquake-prone regions owing to their high section modulus, strength and good seismic performance (Yuan F et al., 2018). They also offer favourable ductility, increased fire resistance, and significant energy absorption capacity. Moreover, construction time and costs can be reduced because CFST columns do not require formwork, and the confinement they provide makes them more rigid than hollow steel tube columns (Ahiwale D et al., 2020).

However, these advantages are offset by some limitations. Seismic actions can cause severe damage in the plastic hinge zone of concrete-filled steel tubular (CFST) columns, such as localised buckling of the steel tubes and crushing of the concrete core. Despite the many cross-sectional configurations proposed for CFST columns, the concrete core is often severely damaged during intense seismic activity, complicating post-earthquake maintenance. (Zhang Z., 2024). Furthermore, given the growing reliance on these structures, it is important to acknowledge that exposed steel tubes are highly susceptible to corrosion, posing a potential threat to their long-term durability and safety (Li W et al., 2024).

Despite their many advantages, tubular columns are complex structural elements whose behaviour remains poorly understood. Although they have many advantages, tubular columns remain complex structural elements whose behaviour is not yet fully understood. Several factors significantly influence their performance. Therefore, further research is required to improve their performance and ensure their long-term durability by understanding their behaviour under different conditions.

In this context, this study examined their structural behaviour to ensure optimal use, drawing on previous experimental, analytical, and numerical

studies to evaluate the performance of this column type.

Figure 1. CFST columns in various types of modern structures. (L.-H Han et al., 2014).

1. FACTORS IMPACTING THE PERFORMANCE OF CFST

1.1 Geometric Parameters

Cross-sectional shape

Research on various CFST column geometries has shown that their structural behaviour depends on their cross-sectional shape. Using square columns can reduce steel usage by up to 30% compared with circular columns (Mohanraj EK et al., 2011). However, the results show that the latter offers better mechanical performance, with lower deflection, higher load capacity, and delayed buckling compared to square columns. In fact, square columns have a lateral load-bearing capacity that is 7.22% lower than that of circular columns (Thirumalai R et al., 2016). Simultaneously, Wang R et al. (2012) showed that CFST columns with hexagonal and octagonal cross-sections behave similarly to square columns, although their structural performance is slightly improved. Three-dimensional finite element models were developed and validated against experimental results for failure modes, load-deformation curves, and ultimate loads for various section types, including circular, triangular, fan-shaped, D-shaped, quarter-circle, and semicircular sections.

The results suggest that CFST (Concrete-Filled Steel Tube) columns with special geometries, when loaded axially, exhibit failure behaviours and load-deformation responses similar to those observed for SHS (Square Hollow Section) or RHS (Rectangular Hollow Section) test specimens (Wang F.-C & Han L.-H, 2018). Other shapes have also been explored. These include steel tubes with elliptical or oval cross-sections (Uenaka K, 2014).

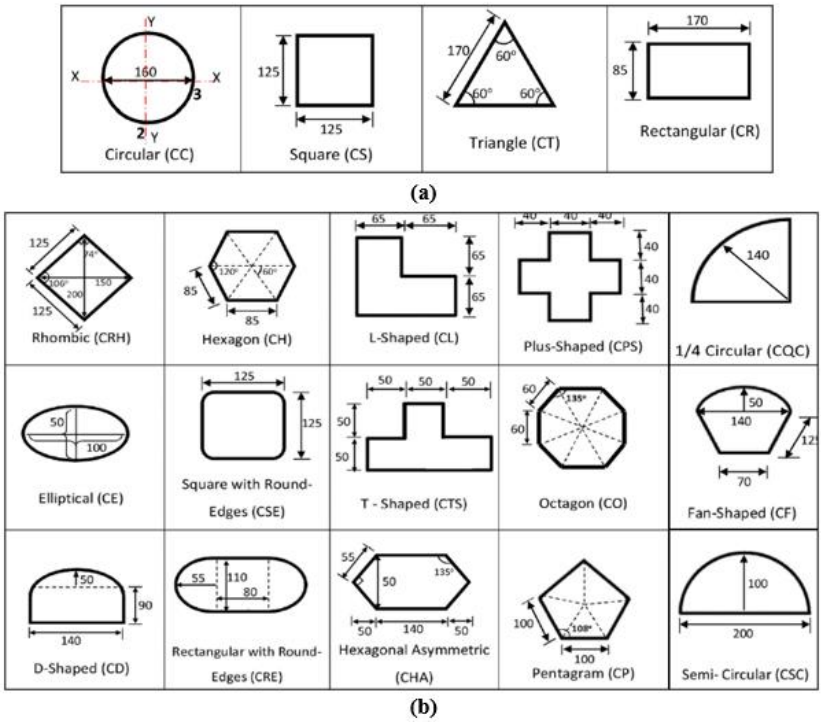

Figure 2. CFST Section **a:** Conventional **b:** Special. (Almamoori AHN et al., 2020).

Slenderness Ratio

The diameter-to-thickness ratio is the ratio of a steel tube's outer diameter to its thickness. This ratio significantly affects the performance of concrete-filled tubular columns: an increase in diameter or a decrease in thickness makes the column slender, reducing its axial capacity. The results show that the maximum stress, maximum strain, plasticity index, and strength index all decrease as the diameter increases. In contrast, the composite elastic units remain relatively constant across different sample dimensions.

Under the maximum load, the vertical stress in the steel tube increased, whereas the hoop stress decreased as the D/t ratio increased. Compared to samples with a small D/t ratio, the vertical stress in the steel tube with a large D/t ratio is lower, while the hoop stress is higher (Liu J., 2023; Shah SMI & Ganesh GM, 2022). There are two types of failure: local buckling, which is observed in non-slender columns, and global buckling, which is typical of slender columns (Salim NM & Al Khekany AM, 2021).

Furthermore, the results of the parametric analysis confirmed that the ultimate load capacity of a CFST column decreases with an increasing D/t ratio and increases with a decreasing L/D ratio (Tiwary & Gupta, 2022). For a constant diameter, the load-bearing capacity increases significantly as the D/t ratio decreases, which highlights the importance of this parameter in optimally designing CFST columns (Du G et al., 2018).

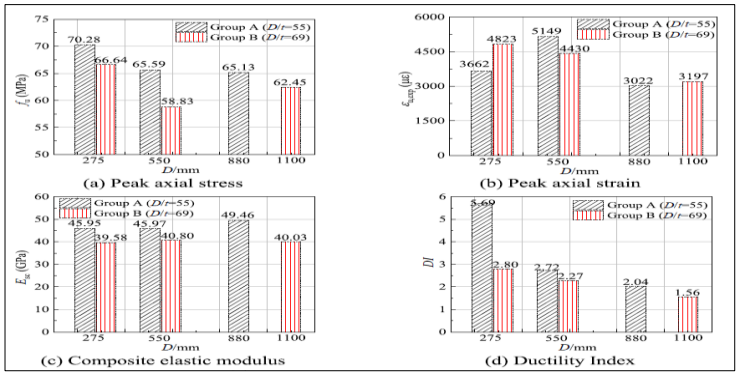

Figure 3. Size Effect on Some Key Performance Indexes. (Liu J., 2023).

1.2 Material Factors

Steel type

Concrete-filled steel tubular elements can be constructed from various types of steel, including normal (mild) carbon steel, high-strength steel and high-performance fire-resistant steel. The properties of steel tubes must comply with standards for steel materials (Han L.-H et al., 2014 [18]). However, Experimental study of the effect of using non-plasticised PVC pipes to confine short concrete columns on their compressive strength.

The study shows greater potential for plastics as a construction material for confining concrete in the near future (Gathimba Naftary K et al., 2014). In contrast to conventional columns, the CFPT specimens exhibited a remarkable energy absorption capacity and continued to undergo deformation after reaching the maximum load. This behavior led to stress softening, producing a gradually descending branch and an enlarged area under the load–deformation curve (Abdulla NA, 2024). Furthermore, although the effect of stainless-steel tube confinement on concrete improvement is slightly less than that of GFRP tubes, it remains effective, particularly in terms of maintaining greater axial deformation when stainless steel is used for the outer shell. (Li YL et al., 2016). In parallel, composite tubular columns made from fibre-reinforced polymer (FRP) and polyvinyl chloride (PVC) have also been used to reinforce concrete. FRP enhances durability, and PVC improves the corrosion resistance of concrete piles in harsh environments (Bazli M et al., 2020; Fakharifar M & Chen GJ, 2017).

Filling Material

Concrete-filled steel tubular elements can be constructed using various types of steel, including normal (mild) carbon steel, high-strength steel, and high-performance fire-resistant steel. The properties of steel tubes must comply with the standards for steel materials (Han L.-H et al., 2014). However, an experimental study was conducted on the effect of using non-plasticised polyvinyl chloride (PVC) pipes to confine short concrete columns on their compressive strength. The study shows a greater potential for plastics as a construction material for confining concrete in the near future (Gathimba Naftary K et al., 2014). In contrast to the conventional columns, the CFPT specimens exhibited remarkable energy absorption capacity and continued to deform after reaching the maximum load. This behaviour leads to stress softening, producing a gradually descending branch and an enlarged area under the load–deformation curve (Abdulla NA, 2024). Furthermore, although the effect of stainless-steel tube confinement on concrete improvement is slightly less than that of GFRP tubes, it remains effective, particularly in terms of maintaining greater axial deformation when stainless steel is used as the outer shell. (Li YL et al., 2016).

In parallel, composite tubular columns made of fibre-reinforced polymer (FRP) and polyvinyl chloride (PVC) have also been used to reinforce concrete. FRP enhances durability, and PVC improves the corrosion resistance of concrete piles in harsh environments (Bazli M et al., 2020; Fakharifar M & Chen GJ, 2017).

Filling Material

Filling steel tubular columns with concrete is one of the most important characteristics of these structural elements. In addition to increasing their load-bearing capacity, this solution is strategic, economical, and environmentally friendly because of the use of solid waste as the filling material. Numerous studies have been conducted on this technique to ensure the structural behaviour and high performance of the columns, while minimising the burdens and costs associated with waste disposal and landfilling. In this context, Mohanraj et al. [7] found that tubular steel columns filled with recycled concrete have a greater maximum load capacity than those filled with conventional or unconfined recycled concrete, while saving approximately 10% of the concrete costs. Therefore, this study proposes an efficient and sustainable solution for solid waste management that is also cost-effective. Furthermore, the experimental results obtained by Tang et al. (2020) showed that CFST columns made from recycled concrete with a high replacement rate of recycled aggregates and a high slenderness ratio exhibited more ductile behaviour. Additionally, the combined effect of the steel tube and concrete depends on the strength of the concrete core (Yang Y et al., 2021). Moreover, the research conducted by Umamaheswari N. and Jayachandran S. A. revealed that the axial load capacity of CFTs is 2.2–5.5 times greater than that of identical hollow sections. The study also found that the confinement of the concrete core in the steel tubes was more effective in CFT columns with a lower diameter-to-thickness ratio and higher steel surface area.

1.3 Loading factors

Axial Loads

Axial loads are among the most studied topics in the field of concrete-filled steel tube (CFST) columns owing to their importance in evaluating the load-bearing capacity of these elements. It has been observed that the axial compressive strength of CFST columns can be significantly improved through lateral confinement, as well as through the interaction between the steel tube and the concrete core. In certain instances, an initial gap exists between the concrete core and the steel tube. This can be attributed to low compression, concrete shrinkage, or insufficient hardening of the concrete core. This study shows that the presence of a gap reduces the axial compressive strength and ductility of concrete-filled steel tube (CFST) columns (Manigandan R & Kumar M,2024).

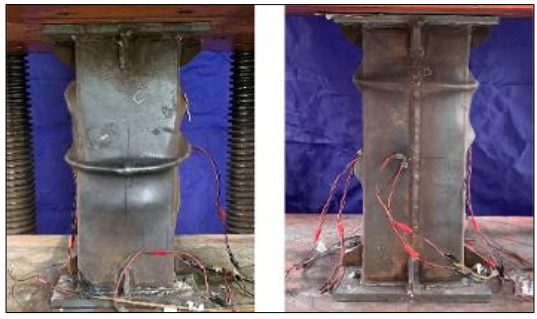

Figure 4. Failure Mode of Specimens CFST (Manigandan R & Kumar M,2024).

Eccentric Loads

Numerous studies have been conducted on the behaviour of concrete-filled tubular columns under eccentric loads, as this factor significantly affects their overall performance. However, an increase in eccentricity reduces the initial strength and stiffness. As the eccentricity and slenderness ratio of the column increased, its initial stiffness and load-bearing capacity decreased, and its bending characteristics gradually became apparent. In contrast to axial compression, the load-strain curve gradually decreased after reaching the maximum strength, and the specimen exhibited ductile characteristics (Lai Z et al., 2024; Zhang R et al., 2020).

The compressive loads on CFST columns under concentric and eccentric conditions were simulated in ABAQUS using experimental data, and a numerical modelling approach was developed. The results show that the response of the model in the plastic zone is significantly affected by the dilation angle and ratio of the second stress variant to the tensile meridian. Furthermore, the contact stress between the steel and concrete was sensitive to the eccentric ratios, highlighting the significant confinement effect exerted by the steel tubes in the analysed structure. (Sarwar JM et al., 2022). Furthermore, Ali et al. (2021) showed that the ultimate strength of the columns decreased as the eccentricity ratio of the load increased. For samples subjected to eccentric compression, global bending occurred first, followed by local buckling of the steel tube surface (Chen A et al., 2025). Moreover, the eccentric compression columns exhibited a failure morphology characterised by progressive lateral deflection from the base to the mid-zone as the wall thickness increased. The ratio between the theoretical ultimate capacity of the columns and the experimental values ranged from 0.35 to 0.94, confirming that the predictive approach was cautious and conservative from a safety perspective. (Wang Y et al., 2023). Mohsen Merwad A et al. have conducted studies showing that under low axial load levels, the critical fracture energy, impact resistance, and impact force increase, while the impact force duration decreases. Conversely, at high axial load levels, the parameters decreased significantly.

Figure 5. Failure Mode of Specimens CFST. (Zhang R et al., 2020).

Lateral Loads

The square- and circular-section columns exhibited notable differences in behaviour when subjected to lateral stress. In square columns, only local buckling occurs, whereas in circular columns, cracks (3 mm crack width) form in the base of the column under lateral loading (ThirumalaiR et al., 2016). Furthermore, the load-displacement curve under lateral loads exhibited a typical elastoplastic tendency. Additionally, the steel casing slightly increases the deformation modulus but reduces the ultimate load-bearing capacity (Wang C et al., 2018).

Figure 6. Failure Mode of Specimens CFST. (Thirumalai R Et Al., 2016).

Cyclic Loads

Numerous studies have focused on the behaviour of concrete-filled tubular columns under cyclic loads to gain a deeper understanding of their behaviour under this type of load. According to the experimental results of Cao et al. (2021), CFST columns reached the 'collapse prevention' state (4% drift) before the onset of local buckling. In contrast to the typical behaviour under monotonic compression, strength degradation occurred only at an advanced stage, highlighting the favourable ability of CFST columns to prevent collapse under seismic loading. The secant stiffness decreased sharply in response to impulses with a drift amplitude of 4%. The earlier the arrival of the impulses, the greater the drop in the secant stiffness. Impulses near the fault imparted considerable energy to the columns, leading to slow local buckling and gradual strength degradation, but significant stiffness degradation occurred.

Testing structural components under earthquakes near the fault by shifting the impulse cycles to the fifth cycle of a conventional cyclic loading history was proposed. In addition, Cao et al. (2019) found that concrete-filled steel tube columns failed by buckling and retained their shape under cyclic axial compression, similar to samples subjected to monotonic loading. Cyclic axial loading slightly reduced the peak stress by approximately 2%–3% but increased the corresponding strain by 25%. The loading and unloading moduli in the post-peak stress phase were approximately 70% and 85% higher than the initial moduli, respectively, owing to the improved interaction and confinement resulting from the initial loading cycle. Furthermore, the absorbed energy depended strongly on the strain and confinement, while being minimally affected by the cyclic loading histories. Lee et al. (2014) demonstrated that the stress deterioration rate is not affected by the confinement coefficient or loading patterns. Furthermore, the concept of ignoring the effect of loading history on the permanent axial strain of concrete during unloading and reloading is invalid, as repeated cycles of unloading and reloading have a cumulative effect on permanent strain and stress deterioration.

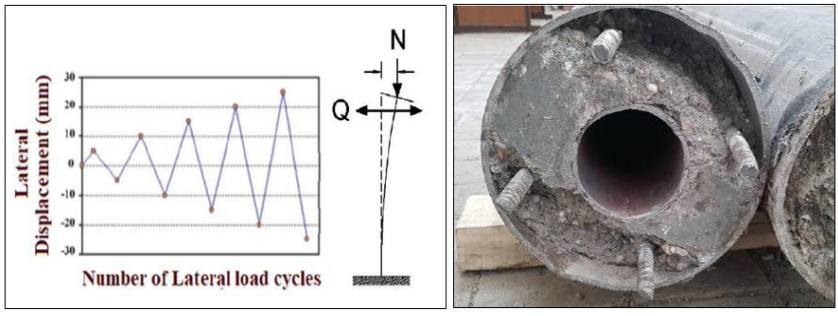

Figure 7. Failure Mode of Specimens CFST. (Faramarzzadeh V et al., 2024).

1.4 Environmental Factors

High Temperature

Several studies have examined the effects of increased temperature on the performance of concrete-filled tubular columns to evaluate their fire resistance. Tests show that increasing the temperature across the cross-section of CFST columns significantly reduces their residual axial load-bearing capacity and axial stiffness compared with unheated columns.

Comparing the axial compressive capacities of square and circular CFST columns made of the same concrete material showed that the circular column exhibited slightly better post-fire structural behaviour than the square column (Kamani F et al., 2020). Mirmomeni et al. 2017, investigated whether partially damaged concrete and composite elements could withstand additional stresses in the event of a subsequent fire. The damaged specimens were exposed to high temperatures, and their residual mechanical properties were measured using a quasi-static compression test. The results suggest that the variation in the residual properties of partially damaged concrete and composite elements depends on the level of pre-damage and exposure temperature. The effect of pre-deformation was less significant at very high temperatures. Moreover, exposure to fire significantly reduces the bond strength between the steel tube and concrete core, primarily because steel expands more rapidly than concrete when heated. This differential expansion can create a gap between the two materials at temperatures as low as 200°C, reducing the confinement effect and exacerbating load-bearing capacity losses (Song T Y et al., 2017).

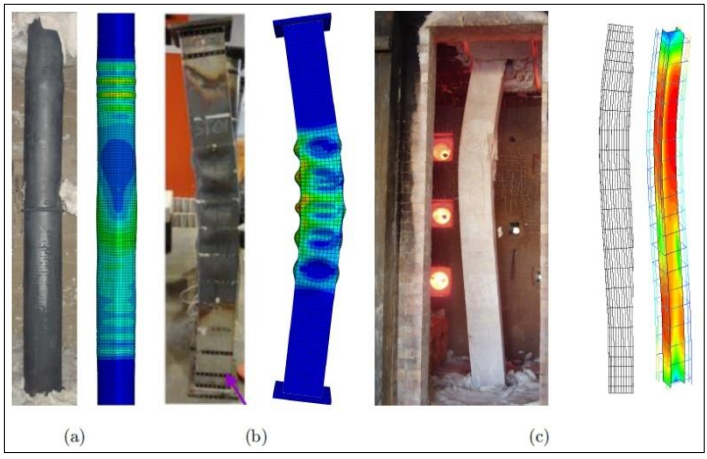

Figure 8. Failure Mode of Specimens CFST. (Tan Q et al., 2018).

Corrosion

Corrosion is the main factor affecting concrete-filled tubular columns, altering their behaviour and reducing their load-bearing capacity, especially in aggressive environments.

Corrosion of steel in concrete-filled steel tubes (CFSTs) leads to structural deterioration, and any extreme action on a corroded CFST poses a serious threat to its integrity. Localised pitting corrosion results in more severe deterioration of CFST behaviour in the event of lateral impact, due to the concentration of plastic deformation, weakened confinement, and reduced energy-absorption capacity of the steel tube (Li G et al., 2023). Zheng et al. (2023) revealed that the axial load supported by the steel tube decreased by 8.1–41.3% as the corrosion rate increased from 0% to 30%. In other cases, this can be interpreted as indicating that the impact of the steel tube on the confining force and sectional axial force diminishes as chloride corrosion progresses. This is linked to the degradation of mechanical properties and the reduction in the steel's adequate thickness. Furthermore, corrosion not only causes a loss of wall thickness but also significantly decreases the yield strength, modulus of elasticity, and tensile deformation capacity of the steel sections. It also substantially deteriorates the load-bearing capacity, ductility, and energy dissipation of CFST columns. The higher the axial force ratio, the greater the deterioration in the deformation capacity of the columns (Yuan F et al., 2018).

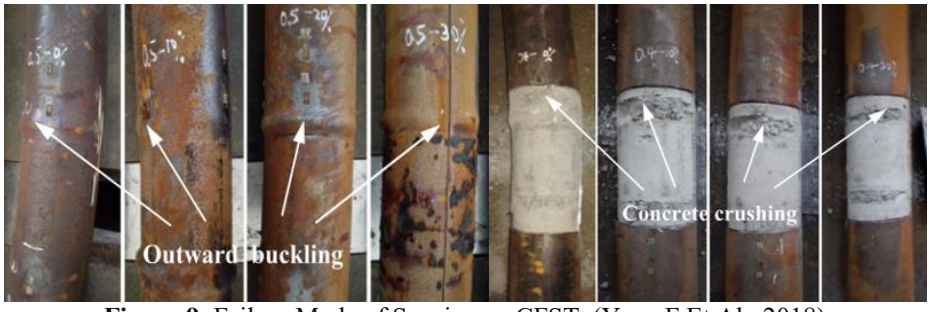

Figure 9. Failure Mode of Specimens CFST. (Yuan F Et Al., 2018).

CONCLUSION

This study facilitated a comprehensive examination of the principal factors affecting the performance of concrete-filled tube columns. These factors include geometric slenderness, cross-sectional shape, filling type, loading conditions, heat exposure, and corrosion. These elements significantly contribute to the capacity and collapse mechanisms of columns.

The findings indicate that the behaviour of these columns cannot be attributed to a single factor but rather to the intricate interaction of multiple factors, particularly the interaction between steel and concrete under varying stresses. Despite substantial advancements in experimental studies and numerical modelling, knowledge gaps persist, especially regarding the impact of interdependent environmental factors, such as corrosion and high temperatures, and the application of modern environmentally friendly composite materials. Enhancing our understanding of these factors will enable us to improve the robustness, durability, and efficiency of structural systems over the long term.

REFERENCE

Abdulla NA. The behavior of concrete-filled plastic tube specimens under axial load. *Jordan Journal of Civil Engineering* 2020;14(1):164–174.

Ahiwale D, Khartode R, Bhapkar A, Narule G, et Sharma K. Influence of compressive load on concrete filled steel tubular column with variable thickness. Innovative Infrastructure Solutions 2021;6(1):1-14. https://doi.org/10.1007/s41062-020-00390-z

Ahmed A D, et Güneyisi E M. Structural performance of frames with concrete-filled steel tubular columns and steel beams: Finite element approach. Advanced Composites Letters 2019; 28:1–15. https://doi.org/10.1177/2633366X19894593

Ali RB, Islam MM, Begum M, Rahman MS. Behavior of concrete-filled steel tubular cold-formed built-up slender square columns under eccentric compression. Innovative Infrastructure Solutions 2021;6(4):189. https://doi.org/10.1007/s41062-021-00552-7

Almamoori AHN, Naser FH, Dhahir MK. Effect of section shape on the behaviour of thin-walled steel columns filled with light weight aggregate concrete: Experimental investigation. Case Studies in Construction Materials 2020;13: e00356. https://doi.org/10.1016/j.cscm.2020.e00356

Bazli M, Bazli L, Rahmani R, Mansoor S, Ahmadi M, Pouriamanesh R. Concrete filled FRP–PVC tubular columns used in the construction sector: A review. Journal of Composites and Compounds 2020;2(4):155–162. https://doi.org/10.29252/jcc.2.3.7

Cao VV, Le QD, Nguyen PT. Experimental behaviour of concrete-filled steel tubes under cyclic axial compression. Advances in Structural Engineering 2019;23(1):74–88. https://doi.org/10.1177/1369433219866107

Cao VV, Vo CT, Nguyen PT, Ashraf M. Experimental behaviour of circular concrete-filled steel tubular columns under lateral cyclic loadings. Earthquakes and Structures 2021;21(5):445–460. https://doi.org/10.12989/eas.2021.21.5.445

Cao VV. Experimental behavior of circular concrete-filled steel tubular columns under near-fault cyclic loadings. Structures 2023; 52:449–463. https://doi.org/10.1016/j.istruc.2023.04.011

Chen A, Li W, Wang H, Yuan L. Study on the mechanical behaviour of multicell T-shaped concrete-filled steel tubular short columns under axial and eccentric compression. Advances in Structural Engineering 2025; 28:1-19. https://doi.org/10.1177/13694332251319097

Du G, Andjelic A, Li Z, Lei Z, Bie X. Residual axial bearing capacity of concrete-filled circular steel tubular columns (CFCSTCs) after transverse impact. *Applied Sciences* 2018;8(5):793. https://doi.org/10.3390/app8050793

Fakharifar M, Chen GJ. FRP-confined concrete filled PVC tubes: A new design concept for ductile column construction in seismic regions. Construction and Building Materials 2017;130:1–10. https://doi.org/10.1016/j.conbuildmat.2016.11.056

Faramarzzadeh V, Ferdousi A, Zandi Y. Cyclic behavior of concrete-filled double steel tubular column with new reinforced circular cross-section. Research Square (preprint) 2024. https://doi.org/10.21203/rs.3.rs-4313317/v1

Gathimba Naftary K, Oyawa Walter O, Mang'uriu Geoffrey N. Compressive strength characteristics of concrete-filled plastic tubes short columns. *International Journal of Science and Research* 2014;3(9):2168–2174. https://doi.org/10.21275/ART20193144

Han L.-H, Li W, Bjorhovde R. Developments and advanced applications of concrete-filled steel tubular (CFST) structures: Members. Journal of Constructional Steel Research 2014; 100:211–228. https://doi.org/10.1016/j.jcsr.2014.04.016

Han L.-H, Li W, Bjorhovde R. Developments and advanced applications of concrete-filled steel tubular (CFST) structures: Members. *Journal of Constructional Steel Research* 2014; 100:211–228. https://doi.org/10.1016/j.jcsr.2014.04.016

Kamani F, Bakhtiyar S, Mazroi A, Mirhoseini M. Experimental study of concrete-filled steel tube (CFST) columns after exposure to high temperature. Modares Civil Engineering Journal 2020;20(2):177–188. https://doi.org/10.1001.1.24766763.1399.20.2.14.2

Lai Z, Huang J, Yang X, Yan J, Shi Y, Zhang C. Eccentric compressive behavior and design of high-strength CFST columns with embedded GFRP tubes. Engineering Structures 2024; 320:118903. https://doi.org/10.1016/j.engstruct.2024.118903

Lee HP, Awang AZ, Omar W. Effect of confining layers of steel straps on high-strength concrete under uniaxial cyclic compression. Construction and Building Materials 2014; 72:48-55. https://doi.org/10.11113/jt.v70.2384

Li G, Hou C-C, Shen L, Hou C-C. Lateral impact behaviour of concrete-filled steel tubes with localised pitting corrosion. Steel and Composite Structures 2023;47(5):615–631. https://doi.org/10.12989/scs.2023.47.5.615

Li W, Zhu M, Li G, Hu Y, Wang B, Cao Y, He W, Li H, Tang Z, et Zhang Y. Influence of compressive strength and steel-tube thickness on axial compression performance of ultra-high-performance concrete-filled stainless-steel tube columns containing coarse aggregates. Buildings 2024;14(11):3605. https://doi.org/10.3390/buildings14113605

Li YL, Zhao XL, Raman Singh RK, Al-Saadi S. Experimental study on seawater and sea sand concrete filled GFRP and stainless steel tubular stub columns. *Thin-Walled Structures* 2016; 106:390–406. https://doi.org/10.1016/j.tws.2016.05.014

Liu J, Gao P, Lin X, Wang X, Zhou X, Chen YF. Experimental assessment on the size effects of circular concrete-filled steel tubular columns under axial compression. *Engineering Structures* 2023; 275:115247. https://doi.org/10.1016/j.engstruct.2022.115247

Manigandan R, Kumar M. Effect of imperfection on behaviour of axial loaded square and rectangular concrete-filled steel tubular columns. Structures 2024; 60:105931. https://doi.org/10.1016/j.istruc.2024.105931

Mirmomeni M, Heidarpour A, Zhao XL, Packer JA. Effect of elevated temperature on the mechanical properties of high-strain-rate-induced partially damaged concrete and CFSTs. International Journal of Impact Engineering 2017; 110:346–358. https://doi.org/10.1016/j.ijimpeng.2017.02.006

Mohanraj EK, Kandasamy S, Malathy R. Behaviour of steel tubular stub and slender columns filled with concrete using recycled aggregates. Journal of the South African Institution of Civil Engineering 2011;53(2):31–38

Mohsen Merwad A., El-Sisi A.A., Sallam H.E.-M., Abu-Barakat S. Transverse impact on hollow and concrete filled steel tubular members: An overview. Egyptian International Journal of Engineering Sciences and Technology 2020; 32:49–58. https://doi.org/10.21608/eijest.2021.53931.1031

Salim NM, Al-Khekany AM. Experimental Evaluation of Slenderness Ratio of Composite Column Reinforced by Multi-skin Steel Tubes. Arabian Journal for Science and Engineering 2021. https://doi.org/10.1007/s13369-021-05848-5

Sarwar JM, Pal A, Ibrahim I, Mustafy T. Numerical Modelling of Concrete-Filled Steel Tube Columns Under Eccentric Loading. Lecture Notes in Civil Engineering 2022; 215:221–240. https://doi.org/10.1007/978-981-16-7924-7_14

Shah SMI, Ganesh GM. Impact of diameter to thickness (D/t) on axial capacity of circular CFST columns: Experimental, parametric and numerical analysis. *International Journal of Applied Science and Engineering* 2022;19(2):2021486. https://doi.org/10.6703/IJASE.202206_19(2).005

Song TY, Tao Z, Han LH, Uy B. Bond behavior of concrete-filled steel tubes at elevated temperatures. Journal of Structural Engineering 2017;143(11):04017147. https://doi.org/10.1061/(ASCE)ST.1943-541X.0001890

Tan Q, Gardner L, Han LH. Performance of steel-reinforced concrete-filled stainless steel tubular columns at elevated temperature. International Journal of Structural Stability and Dynamics 2018;19(1):1940002. https://doi.org/10.1142/S0219455419400029

Tang Y, Fang S, Chen J, Ma L, Li L, Wu X. Axial compression behavior of recycled-aggregate-concrete-filled GFRP–steel composite tube columns. Engineering Structures 2020; 216:110676. https://doi.org/10.1016/j.engstruct.2020.110676

Thirumalai R, Gobinath S, Deva Prasanth KS, Gowtham P, Gowtham Kumar S. Behaviour of Steel Concrete Composite Columns under Lateral Load.

SSRG International Journal of Civil Engineering 2016;3(11):1–6. https://doi.org/10.14445/23488352/IJCE-V3I11P101

Tiwary, A.K., Gupta, A.K. Axial Loading Behaviour of Concrete Filled Steel Tube (CFST) Columns: A Parametric Study. In: Gupta, A.K., Shukla, S.K., Azamathulla, H. (eds) Advances in Construction Materials and Sustainable Environment. Lecture Notes in Civil Engineering 2022;196. Springer, Singapore. https://doi.org/10.1007/978-981-16-6557-8_71

Uenaka K. Experimental study on concrete filled elliptical/oval steel tubular stub columns under compression. Thin-Walled Structures 2014; 78:131–137. https://doi.org/10.1016/j.tws.2014.01.009

Umamaheswari N, Jayachandran SA. Influence of Concrete Confinement on Axial Load Capacity of Concrete-filled Steel Tubes. Journal of Civil Engineering Research 2014; 4:12–16. https://doi.org/10.5923/c.jce.201401.03

Wang C, Liu X, Li P. Experimental Behavior of Concrete-Filled Steel Tubular Members Subjected to Lateral Loads. Advances in Materials Science and Engineering 2018; 2018:9065378. https://doi.org/10.1155/2018/9065378

Wang F.-C, Han L.-H. Analytical behavior of special-shaped CFST stub columns under axial compression. Thin-Walled Structures 2018; 129:404–417. https://doi.org/10.1016/j.tws.2018.04.013

Wang R, Han L.-H, Hou C.-C. Behaviour of concrete filled steel tubular (CFST) members under lateral impact: Experiment and FEA model. Journal of Constructional Steel Research 2012; 80:188–201. https://doi.org/10.1016/j.jcsr.2012.09.003

Wang Y, Sun S, Zhang L, Jia Y. Strength Behavior and Ultimate Capacity Prediction of Self-Compacting Concrete-Filled Thin-Walled Medium-Length Steel Tubular Columns under Eccentric Compression. Buildings 2023;13(11):2876. https://doi.org/10.3390/buildings13112876

Yang Y, Wu C, Liu Z, Qin Y, Wang W. Comparative study on square and rectangular UHPFRC-filled steel tubular (CFST) columns under axial compression. *Structures* 2021; 34:2054–2068. https://doi.org/10.1016/j.istruc.2021.08.104

Yuan F, Chen M, Huang H, Xie L, et Wang C. Circular concrete filled steel tubular (CFST) columns under cyclic load and acid rain attack: Test simulation. Thin-Walled Structures 2018; 122:90–101. https://doi.org/10.1016/j.tws.2017.10.005

Yuan F, Chen M, Huang H, Xie L, Wang C. Circular concrete filled steel tubular (CFST) columns under cyclic load and acid rain attack: Test simulation. Thin-Walled Structures 2018; 122:90–101. https://doi.org/10.1016/j.tws.2017.10.005

Zhang R, Chen SM, Gu P, Huang Y. Structural behavior of UHPC filled steel tubular columns under eccentric loading. Thin-Walled Structures 2020; 156:106959. https://doi.org/10.1016/j.tws.2020.106959

Zhang Z, Guo X, Yang Z, Zhou Y, Chen K, Sun Q, et Tian P. Experimental investigation on the seismic performance of square concrete/ECC filled stiffened high-strength steel tubular columns. Engineering Structures 2024; 314:118341. https://doi.org/10.1016/j.engstruct.2024.118341

Zheng J, Xu Q, Wang W, Zheng Z, Hou M, Lyu X. Compressive behaviour of circular high-strength self-compacting concrete-filled steel tubular (CFST) stub columns under chloride corrosion: numerical simulation. Buildings 2023;14(12):3775. https://doi.org/10.3390/buildings14123775

CHAPTER 3
MITIGATION AGAINST THE IMPACT OF CLIMATE CHANGE ON AGRICULTURAL PRODUCTS BY EXPLORING THE BENEFITS OF IRRIGATION FACILITIES IN SOUTH – WESTERN NIGERIA

S. S. OMOPARIOLA[1]
A. A. ADEALA[2]

[1]Civil Engineering Department The Federal Polytechnic, Ilaro, samuel.omopariola@federalpolyilaro.edu.ng, ORCID ID: 0000-0003-4582-8322
[2]Civil Engineering Department The Federal Polytechnic, Ilaro, adeniran.adeala@federalpolyilaro.edu.ng

INTRODUCTION

Climate change poses increasing risks to agriculture in South-Western Nigeria, including increased drought risk, rising temperatures (1.7–2.5°C by 2050), and unpredictable rainfall (between 11% and 14% predicted under RCP4.5) [1]. These changes put food security and farmer livelihoods at risk by destabilizing yields of staple crops like vegetables, cassava, and maize. In light of this, irrigation becomes a crucial adaptive tactic.

South-West Nigerian agriculture is highly dependent on rainfall, which makes it susceptible to climatic fluctuations. Many farmers always deal with water scarcity throughout the post-rainy season, which lowers productivity and ultimately causes food shortages. South-West Nigerian farmers deal with a number of difficulties, including: (a.) Water scarcity: During the dry season, many places have little access to dependable water supplies. (b.) Budgetary Restrictions: Farmers frequently lack the funds necessary to make irrigation infrastructure investments. (c.) Infrastructure Problems: Access to markets and resources is hampered by inadequate road networks and a dearth of storage facilities. (d.) Knowledge gaps: Inadequate access to instruction and data regarding irrigation techniques Ojezele O. J. (2024). Farming has used irrigation practically from the beginning of time. Egypt and the Nile River back then are examples of this. Only locations near rivers are suitable for irrigation. Using a borehole as an irrigation source could not yield the expected outcome. Although I believe that irrigation can support the nation's seasonal agricultural, the best way to ensure food security is to address insecurity issues permanently. For smallholder farmers, the cost of purchasing electricity will be high. Ogunnaike, E. (2024)

This study investigates how South-West Nigerian agriculture can be protected from climatic shocks by using climate-smart irrigation, which includes drip, sprinkler, and solar-powered systems. It looks at the water resources in the area, identifies obstacles to adoption, and suggests legislative measures to increase the use of water-efficient technologies. In one of Nigeria's most vulnerable agro-ecological zones, irrigation provides a practical route to climate resilience, increased productivity, and poverty reduction by improving water security and facilitating year-round farming.

1. CHARACTERISTICS OF THE VEGETATION OF SOUTH WESTERN NIGERIA

The vegetation of South Western Nigeria can be categorized into several zones. These include: mangrove swamp forest, freshwater swamp forest, rain forest, guinean savannah and montane vegetation.

Mangrove Swamp Forest: This type of vegetation is predominant in the coastal areas of Lagos, Ogun and Ondo State. Its characteristic is dependent on the influence of salt water which results in poor soil quality. Stabilized area of this type of vegetation is very suitable for rice cultivation. The types of plants that can be planted in this zone are plants that are resistant to harsh adaptable environments and can tolerate saline water, withstand water logging, and brackish conditions. Such crops include rice, coconut, cocoa, banana, plantain sweet potato, cassava, yam and fruits (Numbere and Camilo (2016); Numbere (2018), Ita *et. al.* (2019)).

Freshwater Swamp Forest: This type is located in Lekki conservation area of Lagos state, river basin area of Ogun state and in the lower parts of Ondo State. The zone has diverse and productive species. It provides suitable habitats for plants and rare wildlife. It is also very suitable fish farming because of its freshwater characteristics. Crops that can be planted in thi zone are slightly different from that of the mangrove swamp forest. They consists of most of the above and includes plants that cannot withstand the salty mangrove water such as maize, cocoyam, sugarcane and vegetable (Ogunlade and Aikpokpodion (2019).

Rainforest: The rainforest is situated across all the six states of the South Western region comprising of Ekiti, Lagos, Ogun, Ondo, Osun and Oyo States. It is characterized by dense forest populated with considerable proportion of mountainous multi-tiered tropical forests with tall tress some of which ranges between 40 – 45 meters tall. It also consists of dense foliage, heavy epiphytes, shade tolerant shrubs, palms and seedlings. Other constituents are herbs, ferns and thick leaf litters. It supports the growth of cash crops such as cocoa, cashew, kolanut, oil- palm, coffee, plantain and rubber.

Common food crops grown in this zone includes yam, cassava, maize, melon and fruits such as citrus, mango, pawpaw, avocado (Ogunlade and Aikpokpodion (2019), Okoye *et. al. (2019,* Nwakor F.N., et. al. (2019), Adeoye et.al, Omoregie et.al. (2019)

Guinea Savannah: This type of vegetation is more prominent in the North Central region of Nigeria. However, it is present in some areas of South Western Nigeria. It is characterized by moist guinea grassland. This zone does not support the growth of cash crops like cocoa, kolanut etc. but the growth of plants like maize yam, cassava, sorghum, millet, cowpea, groundnut, soybeans, rice and vegetable (Olaniyan et. al. (2018), Akinpelu (2018), Ogunniyi et. al., (2019) Kamara (2018)).

Montane Vegetation: This zone is typically found in high-mountain areas predominant in Ekiti state and some parts of Osun and Ondo States. It is characterized by open grassland with medium sized trees of heights ranging between 10 – 15 meters scattered here and there in the terrain. Predominant crops grown in this zone are carrot beans, maize, potatoes and vegetables. (Okafor (2018), Adepoju et. al. (2019), Akinpelu (2018), Ogunniyi (2018))

2. RAINFALL PATTERN IN SOUTH WESTERN NIGERIA

The pattern of rainfall in the South Western region of Nigeria is closely associated with the vegetation of region and these can be broadly classified as Mangrove swamp, fresh swamp, rainforest, guinea savannah and montage rainfall patterns. It is noteworthy to state that the rainfall has great influence on the type of vegetation as well as the agricultural practice of a zone. The various patterns are discussed in the foregoing sections.

Rainfall Characteristics of Mangrove Swamp Forests: The characteristics of rainfall in this zone is to a great extent dependent on a combination of coastal and reverie factors. Due to its nearness to the equator, the total annual rainfall is between 2,000 and 4,000 mm per annum. The seasonal duration of rainfall in the zone consists of a strong wet season (April–October) with peak rains in June–July, followed by a short dry season (November–March). The intensity of rainfall is heavy and can be above 100 mm/day) during the wet season. It is often accompanied with storms and squalls. The humidity is persistently high about 80 - 90 % RH all the year round.

This is because of the tidal flooding and dense canopy offered by the thick forest. The heavy down pour influences both the soil and water quality of the area. This type of rainfall characteristics influences the water quality available for the uptake of agricultural crops. The heavy downpour drives fresh water input and dilutes saline water, this notwithstanding, due to the closeness of the zone to coastal lines, tidal cycles is responsible for pushing salt water inland resulting in the brackish condition of soil water (Numbere and Camilo (2016); Numbere (2018), Ita *et. al.* (2019)).

Rainfall Characteristics of Freshwater Swamp Forests: The freshwater swamp also referred to as inland/flood plains is distinctive in its rainfall pattern. The total annual rainfall is a little bit lower than that of the mangrove forest ranging between 1500 – 3000 mm (60–120 in) per year. The seasonality is the same having a strong wet season (April–October) with peak rains in June–July, followed by a dry season (November–March). The intensity of rainfall as well as the humidity in this zone are equally slightly lower than that of the mangrove forest. The intensity is greater than 80 mm/day, while the humidity is between 70 and 90% RH all the year round because of the dense vegetation and water logging of the zone. Water logging and flooding is a common phenomenon thus providing adequate support for the diversity of aquatic life. (Ogunlade and Aikpokpodion (2019).

Rainfall Characteristics of Rainforest: The total annual rainfall of this zone is similar to that of the fresh swamp forest. However, the range is slightly shorter ranging between 1500 – 2500 mm per year. The seasonality can be described as bimodal pattern; it has a long-wet season from March to July and a short-wet season from September to November with a short dry spell in August called the August break. It also has and a longer dry season from December to February. It has a high intensity with heavy downpour ranging between 80 and 150 mm per day in the peak months of rainfall. This is often accompanied by thunderstorm especially at the beginning and end o the rainy season. The humidity of the zone is high, about 80 to 90 % RH all the year round.

The impact of this type of rainfall on the agricultural practice is that dense canopy vegetation is sustained consequently supporting high biodiversity and promoting rapid recycling of nutrient (Ogunlade and Aikpokpodion (2019), Okoye *et. al. (2019,* Nwakor F.N., et. al. (2019), Adeoye et.al, Omoregie et.al. (2019).

Rainfall Characteristics of Guinea Savannah: The total annual rainfall of the zone is in the range of 1000 – 1500 mm per year. It has a uni – modal pattern of seasonality that is a single raining season from April to October with peak rainfall occurring in June to July. This is eventually followed by a distinct dry season that last from November to March. The intensity of rainfall is moderate to heavy of about 60 – 100 mm per day. Like the rainforest zone, thunderstorm is a phenomenon that is associated with rainfall of this zone. The humidity of the zone is relatively high about 70 to 80% RH. It impacts on agricultural practice of the zone is the provision of support for grassland with scattered trees. This makes the zone suitable for planting of crops like maize, yam, cassava, and sorghum (Olaniyan et. al. (2018), Akinpelu (2018), Ogunniyi et. al., (2019) Kamara (2018)).

Rainfall Characteristics of Montane Forest: The rainfall pattern in this zone is similar to that of the rainforest zone. It has a total annual rainfall of 1800 – 3000 mm per year with an average daily intensity of 100 to 200 mm. It is usually accompanied by thunderstorm and mist. Like the rainforest zone, it has a bimodal seasonal pattern of long wet season between March and July, a short-wet season between September and November, a short dry season in August and a longer dry season between December and February. Because of its high elevation and dense vegetation cover, the humidity is consistently high at 80 to 90% RH. Its rich vegetation cover makes it supportive of high biodiversity and the growth of crops like potato, strawberry, and temperate vegetables (Okafor (2018), Adepoju et. al. (2019), Akinpelu (2018), Ogunniyi (2018)).

3. THE CHALLENGE OF CLIMATE CHANGE

According to Amjath-Babu et al and 2016; Clarke et al., 2012, climate change is a global phenomenon that has impacted negatively on diverse areas of human activity especially in the aspects of their socio-economic activities, livelihoods, health, and food security. Chidiebere and Okewo (2025) posited that the potential effect is more adverse in countries that rely on agriculture for their sustenance and development. Of particular concern are rural agricultural practitioners in Sub-Saharan Africa. This has consequently resulted in shortage of food and attendant droop in food security. In order to mitigate against this negative effect, the need for variety of adaptation strategies is recommended.

Simelton et al. (2013), Adebisi-Adelani and Oyesola (2014), and Zake and Hauser (2014)) opined that Sub-Saharan Africa agricultural output is highly dependent on rainfall, putting the value at about 95%. Chidiebere and Okeowo (2025) asserted that the role of the agriculture in driving economic development so as to achieve the Sustainable Development Goals is paramount. To support this assertion, it was further highlighted that the contribution of the agricultural sector to the GDP of Nigeria in Q1 of year 2021 is about 22.35% (NBS, 2021)

According to it has been projected that further climatic transformations that will cause increased aridity, temperature rise and marginal increase in temperature will still take place in subtropical regions of Africa. The major challenge that is envisaged in the South western Nigeria is the complexities due to climate change resulting in potential shift in precipitation patterns. (FAO, 2015) identified climate change as a global concern that is responsible for insecurity in food production. This it was said to be more acute in developing nations of which Nigeria is classified.

3.1 Effect of Climate Change N Agricultural Practice In South Western Nigeria

South Western Nigeria being an agrarian area is greatly affected by the climate change. It is reshaping the agricultural practices of the area. It is impacting on how farmers grow food, the type of crops planted and the plant that is grown. Climate change is forcing farmers to move from traditional, rain fed methods to more resilient, climate smart systems—diversifying crops, adjusting calendars, and conserving water and soil.

The effect of the climate change has resulted in the followings:

Rainfall pattern shifts: The rainfall pattern in the present days is highly unpredictable. Rainfalls are erratic as a result of late onset, early cessation, and shorter growing seasons.

Farmers now face unpredictable dry spells and intense downpours. The consequence of this is that yields for maize, yam, and cassava have been considerably reduced (Abegaz and Wims (2015), Abid et. al..(2015)).

Temperature rise: The rise in temperature has resulted in increase evapotranspiration which in turn is responsible for stressing of crops and livestock. The consequence therefore is that heat sensitive varieties of crops are grossly affected. This in turn make farmers to shift to more heat tolerant seeds (Abid et. al.. (2015), Adebisi – Adelani and Oyesola 2014)).

Economic toll: Due to reduced crop yield, losses are inevitable and this translates to lower farm income and higher food prices. In the study by 4 an estimated drop of about 5 to 7 % in major crop production giving rise to increase in prices up t 10 t 15 % by 2050 is predicted Ademassu and Kesler (2016)

3.2 Irrigation in South-West Nigeria

Irrigation has been defined as the supply of water to soil for the support of plant growth through artificial means. It is an engineering process to harness and supply water for the enhancement of plant growth where there is low amount of moisture in the soil which can cause the plant to wither. It involves exploitation and storage of water from different sources in reservoirs canals or head works for final distribution to agricultural fields. It also involves in the design of facilities for the collection of water, connection with river control, drainage of waterlogged areas and distribution of water to areas where it is required. Out of the various mitigation strategies for combating the negative effect of climate change, Irrigation practice is the most sustainable means. It is the best option and it becomes imperative in the present moments due to the erratic rainfall being experienced in this part of Nigeria. Additionally the late onset and early cessation of rain, shorter growing seasons and longer dry spells make irrigation a better alternative. This will guarantee stabilized crop yields and let farmers plant high value crops all the year round.

Reasons for Irrigation

The following are the reasons why irrigation is being practiced

- Less Rainfall: - Artificial supply of water becomes necessary when the total rainfall is less than the required amount for plant growth and fruitfulness. Irrigation facilities can be put in place for regular and controlled supply of water to the less disadvantage area.
- Non – Uniform: - Irrigation method can be used to provide water to crops to prevent irregular supply of water in areas where rainfall may not be uniform on the crop period. It can happen that supply of water might be more during the early-stage rain may be more, but no water may be available at the time of flowering and fruition.
- Unreliable Rainfall: Late onset, early cessation, or long dry spells has adverse effect on rain-fed farming. Regular supply of water from irrigation facilities provides a lee way at such instances.
- Commercial Crops with Additional Water: Some commercial crops need additional supply of water because the rainfall in a particular area may be sufficient to raise the usual crops, but may not be sufficient to raise such commercial and cash crops.
- Controlled Water Supply: There are certain crops such as tomatoes that needs controlled amount of water for productive fruition. Such crops need the construction of proper distribution system so that the yield of the crop may be increased.
- Boost Yields Irrigation farming ensures consistent soil moisture that lifts productivity and quality of crop.
- Year-Round Production: Some perennial crops can be planted any time during the year. Irrigation enables dry season farming, opening extra income windows.
- Crop Diversification: Irrigation allows high value, water loving crops such as vegetables, fruits, and spices).
- Mitigate Climate Change: Irrigation is an effective means of mitigating climate change by acting as a buffer against increasing drought frequency and temperature rise.
- Improved Nutrient Use: Fertigation is a means of synchronizing fertilizer with water. It is time saving, cutting waste and boosting efficiency.

- Employment & Food Security Irrigation practice generates jobs, stabilizes local food supply and lowers price volatility.

For agricultural crops to grow, irrigation is necessary. It is impractical to rely solely on rain, particularly in Australia where rainfall can be erratic and insufficient. One of the most crucial elements in establishing a profitable agricultural enterprise is selecting the appropriate irrigation system, since overwatering may be equally harmful to crop growth. Encouraging plant development while reducing soil erosion and water loss is the aim of irrigation. You must understand soil, equipment, plant species, and land formation in order to select the best irrigation system.

3.3 Types of Irrigation Systems

Water is moved upward from a water table that is situated some distance below the soil's surface to irrigate it. If the irrigate can devise the means of execution, the inherent advantages make controlled sub-irrigation an appealing fraction. The benefits include the prevention of evaporative losses from wet soil surfaces or open water, as well as the removal of cultivation obstacles brought on by pipelines and ditches. There are two types of subsurface irrigation: artificial subsurface irrigation and natural subsurface irrigation.

The term "natural subsurface irrigation" refers to the topographical and geological factors that enable it. These are almost level areas with an impervious stratum layered between two and seven meters below a deep top soil with extremely high lateral permeability. Spreader ditchers and wells can refresh this useful underground reservoir if the region with this soil profile is large enough. In artificial subsurface irrigation, water is forced through a network of buried, perforated pipes at high pressure so that it seeps into the soil. Only when the soil has limited vertical permeability and great horizontal permeability will this strategy work. These kinds of systems need pipes with depths of about 500 mm and spacing as little as 450 mm. They are costly and susceptible to deep cultivation management. When in use, they need to maintain pressure through gravity or pumping from an elevated storage. Applying irrigation water to crops can be done in a number of ways, including flooding the field's surface, spraying it under pressure, or applying it inside the crops. The common irrigation techniques are listed below.

Water is sprayed directly to the soil's surface using surface irrigation techniques from a channel at the field's upper reach. The crops may get water in border strips, check basins, or furrows. Two essential prerequisites that are crucial to achieving high efficiency in surface irrigation techniques are well-built water distribution systems that offer sufficient control over water supply to the fields and appropriate land preparations that enable even water distribution throughout the field. According to Goulburn Valley irrigation & landscaping (nd), There are five of the most popular kinds of irrigation systems. In selecting an irrigation system (nd) four types irrigation methods were mentioned. They are surface, sprinkler, micro and sub irrigation systems. Some of the types are described below.

Border Irrigation

The land is split up into a number of strips that are 10 to 20 meters broad and 100 to 300 meters long when using the border strip flooding technique. These strips go down the dominating slope or any other appropriate slope and are divided by low levees or borders (low flat dillies). Water from the supply ditch is directed onto the head of the border for irrigation. Water moves toward the lower end of the strip, constrained and directed by two borders in a thin sheet. The approaching sheet of water covers the whole width of the strip since the surface is practically level between two borders.

Check Basin Irrigation

In theory, this is the most straightforward irrigation technique. Although there are several ways to use it, they all entail splitting the field into smaller unit portions such that each has a surface that is almost level. The regions are surrounded by bunds or ridges that create basins where irrigation water can be regulated. By permitting water to continue flowing into the basins, the water depth can be maintained for a substantial amount of time. The basins are filled to the required depth and the water is held there until it seeps into the soil.

Furrow Irrigation

Row crops are irrigated using the furrow method, which involves creating furrows between the crop rows during planting and cultivation.

The crop cultivated, the equipment utilized, and the distance between crop rows all affect the furrow's size and shape. I applied water by creating tiny streams in the spaces between the rows of crops. As seen below, water seeps into the soil and flows laterally to irrigate the spaces between the furrows. The amount of water needed to replace the root zone, the soil's infiltration rate, and the soil's lateral water spread rate all affect how long the water should blow in the furrow. By varying the number of furrows irrigated at any given time to suit the available furrow, both large and small irrigation streams can be utilized.

Drip Irrigation Systems

Drip irrigation systems, which are frequently employed in vineyards, orchards, and high-value food crops, are made up of a network of tubes with tiny holes or emitters. They drip water into the soil gradually over extended periods of time and can be positioned above or below the soil's surface. Drip irrigation, sometimes referred to as trickle irrigation, applies water in the form of droplets very next to the plant's base. Water is delivered to the plant via drop nozzles via a network of flexible pipe lines that run at low pressure. By maintaining the soil, water, and air proportions within the ideal range, this method—also referred to as the "feeding bottle" method—maintains the soil in its most natural state. By maintaining a minimum soil moisture level equal to the field capacity, drip irrigation maximizes savings by limiting the amount of water provided for the plant's consumptive usage. The method allows for precise control over the administration of nutrients and moisture at predetermined intervals. Although drip irrigation was initially developed in Israel, it is currently used in many other nations. The system is fed nutrients (fertilizer solutions) in addition to irrigation water. In order to prevent contaminants from clogging the drippers' tiny openings, water is first filtered.

Sprinkler Irrigation

Sprinkler irrigation systems distribute water in a thin spray to designated regions via a network of pipes. Tree crops benefit greatly from micro sprinklers. They are also less expensive to operate and require less water. Applying water in the form of a spray, similar to regular rain, is the sprinkler method, which is used for garden grass sprinkling.

Sprinkler irrigation's ability to be used in situations where surface irrigation techniques are ineffective is its biggest benefit. When: i. The land cannot be prepared for surface procedures; this approach is more beneficial. ii. Excessive slopes iii. Unpredictable topography iv. Erosive soil v. Excessively permeable or impermeable soil vi. Over sand or gravel, the soil's depth is shallow. In this system, the cost of land preparation and permanent water delivery system of channels or conduct is less. However, there is large initial investment in the purchase of the pumping and sprinkling equipment. Sprinkler system can be classified under three heads: -

- Permanent system
- Semi-permanent system
- Portable system.

Pivot Irrigation

Pivot Irrigation in the Center A central pipe with outlets revolving around a central pivot point powers a self-propelled center pivot irrigation system. Although it is much larger and supported by steel or aluminum towers, it functions similarly to a sprinkler watering system.

Terraced Irrigation

Terrace irrigation is an ancient agriculture practice that still exists today, generally in mountainous regions. A series of steps are cut into the sloped land so that when it rains, the water flows down from the top step down to the succeeding steps retaining the soil nutrients as it goes.

3.4 Factors that Affect the Choice of Irrigation Method

The selection of irrigation techniques is determined by both economic and technical viability. When the conditions are right, surface methods are typically the least expensive to install, so there's little reason to think about alternative options. However, there may be financial reasons to take into account alternative forms of irrigation when growing high-value cash crops, particularly in situations where surface irrigation is not the best option.

Pokhrel (2018) stated that education, access to the technologies, age, size of land, and proximity to an urban area are some of the considerations for the choice of method of irrigation. In the write up of wplawinc.com, (nd) soil type and topography, local weather patterns, type of crops grown, water quality are some of the factors to be considered in selecting appropriate type of irrigation. Some of these factors are discussed in the foregoing sections.

Land Preparation: Too-deep, regular slopes are necessary for surface irrigation. Steep slopes typically prevent surface irrigation in favor of sprinkler or trickle irrigation unless terracing is to be done, which is an expensive procedure. Another crucial factor is the consistency of the land surface. Slopes must be level with no high or low areas for surface irrigation to be effective. Land grading, the extent of which depends on the natural terrain, is necessary to achieve this. Top-soil was decreased by land grading, neither of which improved crop productivity. It should be mentioned that installing sprinkler irrigation at the outset may be less expensive in certain situations because land grading can be a costly process.

Soil Type Variability: The choice of technique is also influenced by the varieties of soil in the irrigation area. Frequent light irrigation is necessary for soils with limited water availability, which is challenging when using surface techniques. Unless surface irrigation runs are extremely brief, soils with a high infiltration rate often waste water due to percolation below the rooting range. Because so many canals are needed, the short runs raise labor costs, waste land, and create mechanization challenges. Engineers find it challenging to schedule irrigation due to soil variability, particularly when multiple types of soil are present in a single area. As a result, sprinkler and trickle irrigation designs can be readily modified to accommodate regions with varying soil types under these kinds of circumstances.

The Amount and Quality of Water: The irrigation technique is also somewhat influenced by the quantity, quality, and cost of the water supply. Although the effective flow can be increased by providing agricultural storage at times when irrigation is not performed, such as at night, surface irrigation is frequently unfeasible in areas with low water flow.

Water must be used as efficiently as possible if the overall amount is small. Surface systems typically do not achieve high efficiency unless distribution canals are lined and design, operation, and administration are of the highest caliber. Surface techniques are typically far less efficient than sprinklers and trickle irrigation. When water contains silt and undesirable substances, like sewage, then sprinkler and trickle irrigation cannot be chosen.

Climate: Sprinklers are typically inappropriate when winds exceed 15 to 20 km/h because the tiny droplets are blown away and the water application pattern is disrupted, leading to low efficiency. Low humidity and high temperatures diminish the effectiveness of sprinkling; however, sprays can relieve water stress in plants and boost development by reducing the atmospheric water demand. Flooding may occur from heavy rain following surface irrigation.

The Crop: Technically, the choice of a surface or sprinkler approach is largely independent of the type of crop being irrigated. Moving pipes and sprinklers can be challenging when working in tall crops. By its very nature, surface irrigation has comparatively lengthy irrigation cycles, which in severe cases will result in the plants losing more growth than they would under short interval sprinkler or trickle method.

3.5 Suggested Adaptation Strategies to Mitigate Against Climate Change in South Western Nigeria

(Aggrawal (2008), Abegaz and Wims (2015), Amijat – Babu et. al. (2016)) have suggested the following measures as adaptation strategies

Crop diversification: It was suggested that crop varieties of short duration such as beans, vegetables etc. should be planted by farmers

Changing planting dates: Farmers should embrace aligning planting season with new rainfall windows.

Improved water management: Soil moisture management strategies such as mulching rainwater harvesting and irrigation practices should be embraced.

Soil conservation: Soil conservation strategy such as planting of cover crops, agroforestry and application of organic manure should be taken into consideration (Aggrawal (2008), Abegaz and Wims (2015), Amijat – Babu et. al. (2016)).

Jeff-Agboola Y. (2024) suggested affordable Irrigation Systems such as low-cost irrigation farming which offers a workable way to lessen the financial burdens of farmers. Farmers can maintain crop cultivation all year round, guaranteeing food security and enhancing their standard of living, by implementing economical and effective irrigation techniques such as practicing irrigation system using reusable plastic containers. It was added that it will be simpler for farmers to engage in irrigated farming by following this method and by training farmers on their use. Low-loss irrigation farming entails the use of straightforward, reasonably priced methods and tools to give crops enough water during dry spells is known as low-cost irrigation farming. Smallholder farmers, who frequently lack the funds for more advanced irrigation systems, are intended to be able to use these techniques. The secret to inexpensive irrigation is to use locally accessible resources and materials to maximize efficiency while minimizing costs.

Other recommendations are inexpensive irrigation techniques that farmers may use, such as drip irrigation, treadle pumps, rainwater collection, bicket and hole irrigation, furrow irrigation, and flood irrigation. It was further stated that, drip irrigation reduces water waste by delivering water straight to plant roots using recyclable materials. Farmers can use inexpensive pipes or discarded plastic bottles to build a basic drip system. The benefits include lower water consumption, ease of setup, and efficacy for small-scale farming. Used plastic bottles can be gathered by farmers, who can then bury them close to plant roots after making tiny holes in the bottom. Water can be poured into these bottles and allowed to slowly seep into the ground. Another alternative, according to Ojezele (2024), are treadle pumps, which are foot-operated pumps that gather water from rivers or shallow wells and direct it to crops via pipes or hoses. It is inexpensive, fuel-free, and simple to use. Treadle pumps can be built locally or purchased by farmers using readily accessible materials. Farmers who have access to adjacent water sources will find these pumps especially helpful. Rainwater harvesting entails gathering and storing rainwater for use during dry spells. It is economical, less reliant on outside water supplies, and eco-friendly was equally suggested. To collect and store rainwater from rooftops or other surfaces, farmers can build up basic systems employing gutters, storage tanks, or barrels.

This water can then be utilized for irrigation during the dry season. Additionally, the bucket and hose irrigation option she described is the conventional approach, which entails manually drawing water from a source with a bucket and utilizing a hose or watering can to administer it directly to plants. It requires very little equipment and is incredibly inexpensive. This technique works well for extremely tiny gardens or plots where more intricate irrigation systems are not required. Furthermore, furrow irrigation, which is directing water from a source to the crops by making tiny channels along the land was also recommended. It works well for row crops, is easy to set up, and requires few materials. In order to let gravity transport water from a higher position to the plants, farmers can create furrows between crop rows. In places with a slight slope, this approach is effective. Although flood irrigation is less water-efficient, it can be employed for crops like rice that do well in water-saturated environments, according to the expert. This approach may not be appropriate for areas with limited water resources when evaluating local water resources because it demands a plentiful supply of water.

CONCLUSION

Western South Nigerian agriculture is at a turning point, with increased climatic hazards necessitating quick adaptation. This paper emphasizes that climate-smart irrigation is a powerful instrument to stabilize yields, protect food security, and strengthen farmer resilience when combined with supportive policies and funding. steps to increase the use of water-efficient technology. In one of Nigeria's most vulnerable agro-ecological zones, irrigation provides a practical route to climate resilience, increased productivity, and poverty reduction by improving water security and facilitating year-round farming. The conclusions are as follows

- Solar-powered drip and sprinkler systems provide effective, scalable solutions for landscapes with limited water resources.
- Irrigation access increases dry-season farming, diversifies sources of income, and reduces poverty. iii. Adoption hurdles can be removed by customized microfinance, agricultural cooperatives, and government subsidies.

- Nigeria needs to give inclusive, climate-resilient water management top priority in order to reap these benefits. It will be crucial to enhance climate information systems, improve extension services, and promote public-private collaborations.
- Scaling irrigation is ultimately a development requirement as well as an agricultural imperative. South-West Nigeria has the potential to transform climate adversity into equitable and sustainable prosperity through prudent water management.
- Adoption obstacles can be removed by customized loans, farmer cooperatives, and government subsidies.

REFERENCES

Abegaz, D.M. and Wims, P. (2015). Extension agents' awareness of climate change in Ethiopia. J. Agric. Educ. Ext., 21, pp. 479-495.

Abid, M. Scheffran, J. Schneider, U.A. Ashfaq, M. (2015). Farmers' perceptions of and adaptation strategies to climate change and their determinants: the case of Punjab province, Pakistan. Earth Syst. Dyn., 6, p. 225.

Adebisi-Adelani, O. Oyesola, O. (2014). Farmers' perceptions of the effect of climate change on tomato production in Nigeria. Int. J. Veg. Sci., 20, pp. 366-373.

Adeoye I.B., Adebayo S.O., Olaniyan A.A. (2019), Yam Production Systems and Constraints in South-West Nigeria, African Journal of Agricultural Research_ 14(23): 1013-1020

Adepoju A.O., Obidiegwu J.E., Okonkwo C.C. Adaptation of Potato Varieties to Highland Conditions in Nigeria, Journal of Crop Improvement 33(2): 210-222

Adimassu, Z. and Kessler, A. (2016). Factors affecting farmers' coping and adaptation strategies to perceived trends of declining rainfall and crop productivity in the central Rift valley of Ethiopia. Environ. Syst. Res., 5. p. 1.

Aggarwal, P. (2008). Global climate change and Indian agriculture: impacts, adaptation and mitigation. Indian J. Agric. Sci., 78, p. 911.

Akinpelu A.O., Adejumo O.A., Oke O.A. (2018), Economic Analysis of Yam Production in Guinea Savannah Agro-Ecological Zone, African Journal of Agricultural Research 13(28): 1417-1425

Amjath-Babu, T.S. Krupnik, T.J. Aravindakshan, S. Arshad, M. and Kaechele, H. (2016). Climate change and indicators of probable shifts in the consumption portfolios of dryland farmers in Sub-Saharan Africa: Implications for policy, Ecological Indicators, Vol 67, Pg 830-838, (https://www.sciencedirect.com/science/article/pii/S1470160X16301340)

Ita RE, Ogbemudia FO, Kekere O, Udo E. C., (2019) Plant species as influenced by soil relations in a mangrove ecosystem of lower IMO river estuary, Niger Delta, Nigeria. MOJ Eco Environ Sci.;4(3):92-98.

Kamara A.Y., Omoigui L.O., Ekeleme F. (2018), Cowpea Production Systems in the Guinea Savannah of Nigeria, Journal of Agricultural Science_ 156(3): 391-400

Numbere A.O (2018), Mangrove Species Distribution and Composition, Adaptive Strategies and Ecosystem Services in the Niger River Delta, Nigeria Chapter in:_ Mangrove Ecosystem Ecology and Function (IntechOpen, 2018)

Numbere A.O., and Camilo G.R. (2016), Reciprocal Transplant of Mangrove (Rhizophora racemosa) and Nypa Palm (Nypa fruticans) Seedlings in Soils with Different Levels of Pollution in the Niger River Delta, Nigeria, Global Journal of Environmental Research 10(1): PP 14 - 21 (2016)

Nwakor F.N., Nwosu K.C., Okoye B.C. (2019), Cassava Value Chain Analysis in Rainforest Zone of Nigeria, Journal of Development and Agricultural Economics_ 11(4): 71-80

Ogunlade M.O., and Aikpokpodion P.O. (2019, Impact of Climate Change on Cocoa Production in Nigeria, Journal of Agricultural Science 11(3), PP 112-121

Ogunnaike, E. (2024) https://tribuneonlineng.com/how-south-west-farmers-can-key-into-low-cost-irrigation-farming-to-prevent-food-shortages/

Ogunniyi L.T., Omotosho O.O., Adepoju A.O. Impact of Climate Change on Sorghum Production in Northern Guinea Savannah, Climate Research_ 78(1): 45-53

Ojezele O. J. (2024) https://tribuneonlineng.com/how-south-west-farmers-can-key-into-low-cost-irrigation-farming-to-prevent-food-shortages/

Okafor J.C., Onyeachusim H.D., Afolayan M. (2018), Domestication and Breeding of Irvingia gabonensis in Nigeria, African Journal of Plant Science_ 12(4): 85-92

Okoye C.B., Onyeneke R.U., Muoneke O.B.(2019), Economic Analysis of Oil Palm Production Systems in South-West Nigeria, Nigerian Journal of Agricultural Economics 9(1) PP 45-55

Olaniyan A.B., Oyekale A.S., Adeyemo T.A. (2018), Maize Production Systems and Technical Efficiency in the Guinea Savannah of Nigeria, Nigerian Journal of Agricultural Economics_ 8(2): 33-44

Omoregie G.K., Oresanya T.O., Ojomo A.O., (2019), Growth Performance of Rubber Plantations in South-West Nigeria, Journal of Forestry Research, 30(2): 321-330

Pokhrel B. K., Paudel K. P**.** and Segarra E, (2018)**,** Factors Affecting the Choice, Intensity, and Allocation of Irrigation Technologies by U.S. Cotton Farmers, Water Volume 10, Issue 6

wplawinc.com, https://wplawinc.com/5-factors-to-consider-when-choosing-an-irrigation-system

CHAPTER 4
DATA-DRIVEN PREDICTION AND EXPERIMENTAL VALIDATION OF LIME-STABILIZED EXPANSIVE CLAY BEHAVIOR: A GA-OPTIMIZED ANN APPROACH

Y. KELLOUCHE[1]
H. GADOURI[2]
B. MEZIANI[3]
W. BOUKHLIFA[4]

[1]Structure, Geotechnics and Risks Laboratory, Hassiba Benbouali Chlef University, Algeria, y.kellouche@univ-dbkm.dz, ORCID ID: 0000-0003-3052-844X
[2]Earth Science Department, Djillali Bounaama Khemis Meliana University, Algeria, hamid.gadouri@univ-dbkm.dz, ORCID ID: 0000-0002-0753-3569
[3]Earth Science Department, Djillali Bounaama Khemis Meliana University, Algeria, brahim.meziani@univ-dbkm.dz, ORCID ID: 0000-0001-7134-1345
[4]Earth Science Department, Djillali Bounaama Khemis Meliana University, Algeria, maltalord355@gmail.com

INTRODUCTION

Expansive clays are widely recognized as a problematic soil type in civil engineering because of their strong sensitivity to changes in water content. Seasonal wetting and drying or local changes in drainage can induce significant shrink–swell cycles, leading to differential heave, cracking and loss of serviceability in pavements, lightly loaded buildings and buried infrastructure. In many regions, including parts of North Africa and the Mediterranean, expansive clays and marls form a substantial part of the near-surface formations, which makes their proper identification and treatment a recurring design issue.

Among the available ground improvement techniques, lime stabilization is one of the most established and widely used methods for mitigating the behavior of expansive clays. When lime is added, short-term reactions such as cation exchange and flocculation–agglomeration reduce plasticity and improve workability, while longer term pozzolanic reactions form cementitious compounds that increase strength and stiffness (Harichane et al., 2011; Gadouri et al., 2017). Numerous experimental studies on lime-stabilized clays and marls report marked reductions in plasticity index and swelling potential, often accompanied by a shift in soil classification towards lower-plasticity domains in the Casagrande chart (Benyahia et al., 2020; Sorsa & Agon, 2022).

At the same time, Proctor compaction tests consistently show characteristic changes in compaction behavior: for lime contents within an appropriate range, the maximum dry unit weight tends to decrease slightly, whereas the optimum moisture content increases, reflecting both the aggregated soil structure and the higher water demand associated with the formation of cementitious products (Bell, 1993; Mir, 2015; Benyahia et al., 2020; Sorsa & Agon, 2022; Sambre et al., 2024). Together, these results underline that chemical stabilization by lime has a direct and systematic impact on the plasticity and compaction parameters of clayey soils, which are precisely the properties targeted in the present modelling framework. In parallel, the last two decades have seen a rapid growth in the use of artificial intelligence (AI) and machine learning (ML) in geotechnical engineering.

Artificial neural networks (ANNs) in particular have been successfully applied to problems such as prediction of unconfined compressive strength, CBR, shear strength and settlement, often outperforming classical regression-based models when the underlying relationships are strongly non-linear. Several studies and reviews have shown that ANNs can efficiently model the behavior of soils stabilized with lime, cement and blended binders, provided that a sufficiently rich experimental database is available (Jeremiah et al., 2021; Tabarsa et al., 2021; Aljanabi & Salih, 2023). In these works, data-driven models have been used not only to estimate strength parameters, but also to explore the influence of mix composition, curing conditions and testing procedures on the mechanical response of stabilized soils, and to support mixture design under performance and sustainability constraints. However, most existing applications still focus on mechanical strength indicators, whereas index and compaction properties such as plasticity index after treatment, maximum dry unit weight and optimum moisture content have received comparatively less attention as primary targets—despite their central role in the design and quality control of lime-stabilized layers.

However, most of the existing ML work on stabilized soils has concentrated on mechanical strength parameters (e.g. UCS, CBR), whereas index and compaction properties—such as plasticity index after treatment, maximum dry unit weight and optimum moisture content—have received less attention as primary outputs, even though they are central in practice. These parameters control compaction specifications, expected workability and, more generally, the engineering performance of lime-stabilized layers.

A second challenge lies in the design of the ANN models themselves. In many studies, network architectures (number of hidden neurons, activation functions, etc.) are chosen by trial-and-error. This approach may lead to sub-optimal performance or unnecessary model complexity. To overcome this limitation, global optimization techniques such as Genetic Algorithms (GA) can be used to automatically search the space of candidate ANN architectures and hyperparameters, while k-fold cross-validation provides a robust framework for estimating internal generalization performance and reducing sensitivity to a particular train–test split.

In this context, the present chapter develops a GA-optimized, cross-validated ANN model to predict three key parameters of lime-stabilized expansive clays, namely the plasticity index after treatment, the maximum dry unit weight and the corresponding optimum moisture content. The model is trained exclusively on a database compiled from published experimental studies on lime-stabilized clays and marls, using three practical input variables available in routine practice: lime content, initial liquid limit and initial plastic limit of the untreated soil. The ANN architecture and main hyperparameters are optimized by a GA, and k-fold cross-validation is used to assess internal performance on the literature-based database. The resulting model is then evaluated by external validation against an independent experimental program carried out on a highly plastic clay sampled along the RN65 road in Algeria, for which Atterberg limits and standard Proctor tests were performed on soil–lime mixtures with different lime contents.

1. BACKGROUND ON LIME-STABILIZED EXPANSIVE CLAYS AND DATA-DRIVEN MODELLING

1.1 Mechanisms and Experimental Behavior of Lime-Stabilized Expansive Clays

When lime is added to a clayey soil, a series of short- and long-term physico-chemical processes takes place. In the short term, dissolution of calcium hydroxide increases the porewater pH and releases calcium ions, which replace exchangeable cations on clay surfaces. This promotes cation exchange and flocculation–agglomeration of clay particles, transforming a dispersed structure into a more open, aggregated fabric. These reactions explain the immediate decrease in plasticity and the improvement in workability often observed on site (e.g. higher plastic limit, lower plasticity index).

Over longer times, the high-pH environment favors the dissolution of silica and alumina from clay minerals. The dissolved species react with calcium to form cementitious products, mainly calcium silicate hydrate (C–S–H) and calcium aluminate hydrate (C–A–H). These products progressively bond particles and aggregates together, increasing stiffness and strength and reducing sensitivity to water.

Microstructural investigations on lime-treated clays and marls consistently report this transition from a loose, clayey fabric to a denser, cemented matrix (Benyahia et al., 2020; Najafian Jazi et al., 2024). Recent experimental studies provide detailed quantitative evidence of these effects. For an expansive clay subgrade in Jimma (Ethiopia), Sorsa and Agon (2022) showed that adding 2–8% hydrated lime leads to a strong reduction in plasticity index, a decrease in maximum dry density and an increase in optimum moisture content, with an optimum around 5% lime for CBR and swelling performance. In north-eastern Algeria, Benyahia et al. (2020) reported that the swelling pressure of N'Gaous expansive marls drops sharply when lime is added and stabilizes beyond a certain lime dosage, an effect associated with the development of C–S–H and related phases identified by XRD and SEM.

More recent works have extended these observations to blended systems and durability aspects. Sambre et al. (2024) showed that combining lime with supplementary binders such as cement or fly ash further reduces swell potential and improves strength and CBR of expansive subgrade soils, confirming the key role of lime in activating pozzolanic reactions in high-plasticity clays. Najafian Jazi et al. (2024) demonstrated that the compressibility and volume-change behavior of lime-stabilized expansive soils also depend on stress history, highlighting the importance of both chemical and mechanical factors in long-term performance.

Overall, experimental programs on expansive clays treated with lime or lime-based binders consistently show a reduction in plasticity index, characteristic changes in Proctor compaction curves with slightly lower maximum dry unit weight $\gamma_{d\max}$and higher optimum moisture content ω_{opt}, a decrease in swell potential and swell pressure, and a progressive increase in strength as curing time increases.

1.2 Artificial Neural Networks and Machine Learning for Stabilized Soils

In parallel, the use of artificial intelligence in geotechnical engineering has expanded considerably. Artificial neural networks (ANNs) are now widely applied to problems where relationships between variables are strongly non-linear and difficult to represent with simple regression models.

A comprehensive review by Jeremiah et al. (2021) shows that ANNs have been successfully used to predict geo-mechanical properties of stabilized clays treated with cement, lime, geopolymers and by-product cementitious materials. For lime- and cement-stabilized soils, many recent studies have focused on strength prediction. Muhmed et al. (2024) developed ANN and simplified regression models to predict the UCS of lime-stabilized soils and reported robust performance of the ANN model. Onyelowe et al. (2024) used multiple ensemble-based ML techniques to estimate the UCS of cohesive soils stabilised with cement and lime at optimal compaction. Ozioko and Eze (2025) combined laboratory testing with several ML algorithms to model CBR and compressibility of lime-stabilized lateritic soil, showing that ML can reliably support design decisions when an adequate dataset is available.

Beyond UCS and CBR, other soil properties have been modelled with data-driven methods. Shah et al. (2024) proposed an automated ML strategy to predict the resilient modulus of stabilized clayey subgrades, while Luo et al. (2025) introduced a hybrid ML and interpretability framework for UCS estimation based on a large database of stabilized soils. Intelligent mixture design and multi-objective optimization have also been explored to tailor stabilized soil mixtures under performance and sustainability constraints (Wang et al., 2024). Despite this rapid progress, relatively few ML studies have treated plasticity index, maximum dry unit weight and optimum moisture content as main outputs, even though these parameters are central for mix design and compaction control in lime stabilization projects. In addition, in many ANN applications the network architecture is still selected by trial-and-error, and internal validation is sometimes based on a single train–test split, which may lead to sub-optimal models or optimistic performance estimates.

To address these limitations, the present chapter develops a GA-optimized, k-fold cross-validated ANN trained on a literature-based database of lime-stabilized clays and marls. The model uses three practical input variables—lime content and the initial liquid and plastic limits of the untreated soil—and targets the prediction of post-treatment plasticity index, maximum dry unit weight and optimum moisture content.

The following sections describe in detail the construction of the database, the ANN–GA–cross-validation framework, and the subsequent external validation on a local expansive clay from the RN65 road project.

2. LITERATURE-BASED DATABASE FOR MODEL DEVELOPMENT

2.1 Compilation of Experimental Data

The ANN model developed in this work is based on a database compiled from previously published experimental studies on lime-stabilized clays and marls. A targeted literature survey was conducted to identify contributions dealing with the stabilization of clayey or marly soils using hydrated lime or quicklime, reporting Atterberg limits and Proctor compaction characteristics for several lime contents, and providing sufficient information on the initial state of the soil, in particular the index properties of the untreated material.

For each selected study, the numerical data were extracted from tables or, when necessary, digitized from clearly readable graphs. Only mixtures for which both the initial Atterberg limits of the untreated soil and the corresponding properties at a given lime content were available were retained. Studies involving blended binders (such as lime–cement or lime–fly ash combinations) were excluded so that the specific effect of lime could be analyzed in a consistent manner.

The composition of the final database is summarized in Figure 1, which lists, for each reference, the number of usable data points and their percentage contribution to the total dataset. As shown in Figure 1, the database contains 100 records collected from several experimental programs. Some studies contribute only a few points, while others provide a larger number of mixtures and test results. This variety of sources is expected to enhance the generalization capability of the model while keeping the database focused on fine-grained, lime-treated soils relevant to pavement and earthwork applications.

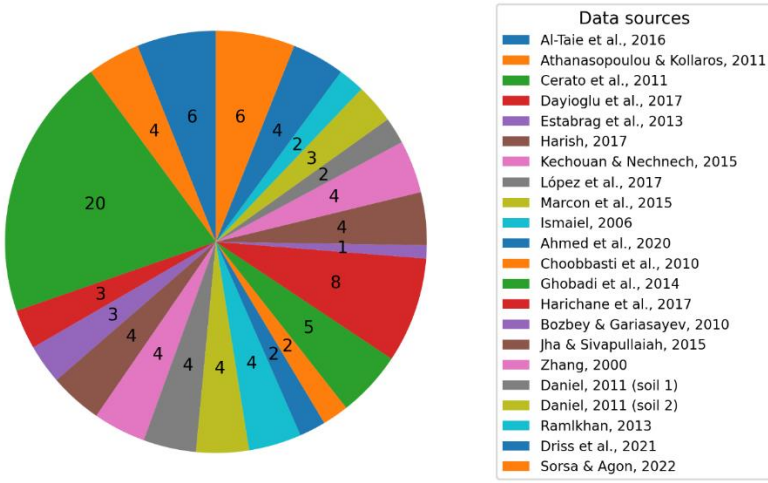

Figure 1. Percentage Distribution of Database Records by Source

2.2 Input and Output Variables

The choice of variables to be used as ANN inputs and outputs was guided by two criteria: practical relevance for design and systematic availability in the literature. As inputs, three quantities were selected: lime content L(%, by dry mass of soil), the initial liquid limit of the untreated soil LL_0(%), and the initial plastic limit of the untreated soil PL_0(%). These parameters are routinely measured in geotechnical investigations and are almost systematically reported in the studies included in Table 1; together, they provide a compact description of the stabiliser dosage and of the plasticity level of the natural soil before treatment. As target outputs, three properties were retained: the plasticity index PI(%), the maximum dry unit weight $\gamma_{d\max}$(kN/m³) obtained from standard Proctor tests, and the corresponding optimum moisture content ω_{opt}(%), which characterises the compaction behaviour of the lime-stabilised mixtures.

These outputs characterize the combined effect of lime on plasticity and compaction behavior, which are key aspects for the design and quality control of lime-stabilized subgrades and base layers. They also complement existing ML studies that have mostly focused on mechanical strength parameters such as UCS or CBR.

2.3 Statistical Ranges and Representativeness of The Data

The information in Table 2 offers a first assessment of the representativeness of the database. The average lime content is about 3.9 %, with a standard deviation of 3.25 % and values ranging from 0 to 12 %. This indicates that most mixtures correspond to low to moderate lime dosages, which are typical of road and earthwork applications, while still covering the upper range used in some experimental studies.

The initial liquid limit (LL_0) has a mean value of approximately 65 %, a median of 68 % and a standard deviation of about 15 %. Together with the initial plastic limit (PL_0) (mean ≈ 28 %, median 29 %, standard deviation ≈ 6.5 %), this confirms that the soils considered are mostly medium to highly plastic clays and marls, consistent with their classification as potentially expansive. The minimum and maximum values (32–115 % for (LL_0) and 19.6–42 % for (PL_0)) show that the database covers a relatively wide spectrum of plasticity levels.

On the output side, the plasticity index (PI) after treatment exhibits a mean of about 23 % and a relatively high standard deviation (≈ 14.6 %), with values ranging from 3 to 78 %. This spread reflects both the diversity of the initial soils and the variation in lime content. The maximum dry unit weight has a mean close to 16 kN/m³ and values between 8.2 and 72 kN/m³, while the optimum moisture content has an average of about 24.8 %, with a minimum of 14.15 % and a maximum of 40 %. These intervals are compatible with the well-known trend of slightly lower maximum dry unit weights and higher optimum moisture contents for lime-stabilized mixes compared with untreated soils.

Although the individual studies compiled in the database differ in terms of testing procedures and material characteristics, the aggregated statistics presented in Table 1 indicate that the dataset is coherent with the qualitative behavior described in Section 2 and is sufficiently broad and consistent to be used for training a global predictive model for lime-stabilized expansive clays.

Table 1. Statistical Parameters of The Database Variables

	Lime (%)	**LL0 (%)**	**PL0 (%)**	**PI (%)**	**γ_{dmax} (kg/m^3)**	**ω_{opt} (%)**
Mean	3.89	65.26	27.77	23.16	16.04	24.82
Median	4	68	29	19.89	15.46	22.56
Standard-deviation	3.25	15.40	6.50	14.56	6.38	6.67
Sample variance	10.56	237.07	42.27	212.06	40,66	44,45
Minimum	0	32	19,6	3	8.2	14.15
Maximum	12	115	42	78	72	40
Sum	404.5	6787.2	2888.18	2408.41	1668.37	2580.8
Sample size	103	103	103	103	103	103

2.4 Distribution of The Input Variables

In addition to the global statistics reported in Table 1, the distribution of the three input variables was examined in order to obtain a more detailed picture of the coverage of the database. Figure 2 displays the histograms of the raw (non-normalized) values of lime content L, initial liquid limit $LL_0$and initial plastic limit PL_0 The histogram of lime content, Figure 2(a), shows that the majority of mixtures correspond to low to moderate lime dosages, typically between a few percent and about 8–10 %, whereas very high lime contents are less frequently reported. This reflects common practice in lime stabilization, where dosages are generally chosen close to the optimum range identified in experimental studies.

The distributions of $LL_0$and PL_0, Figures 2(b) and 2(c), confirm that the database is dominated by medium to highly plastic soils. Most values of $LL_0$are concentrated around the mean and median reported in Table 1, with fewer observations at the lower and upper ends of the range (32–115 %). A similar pattern is observed for PL_0, where the bulk of the data lies close to the central part of the interval 19.6–42 %. This concentration around intermediate plasticity levels is consistent with the fact that many published studies focus on clays and marls that are problematic in practice but still representative of typical subgrade conditions. These distributions indicate that the database provides reasonable coverage of the domain of interest, while also highlighting some degree of skewness and unequal sampling density across the ranges of the input variables.

In particular, mixtures with very low or very high lime contents and extremely low or extremely high plasticity indices are comparatively scarce. This observation motivates the use of an appropriate normalization and scaling procedure for all variables before ANN training, so that the learning process is not biased by differences in magnitude or by the non-uniform spread of the raw data.

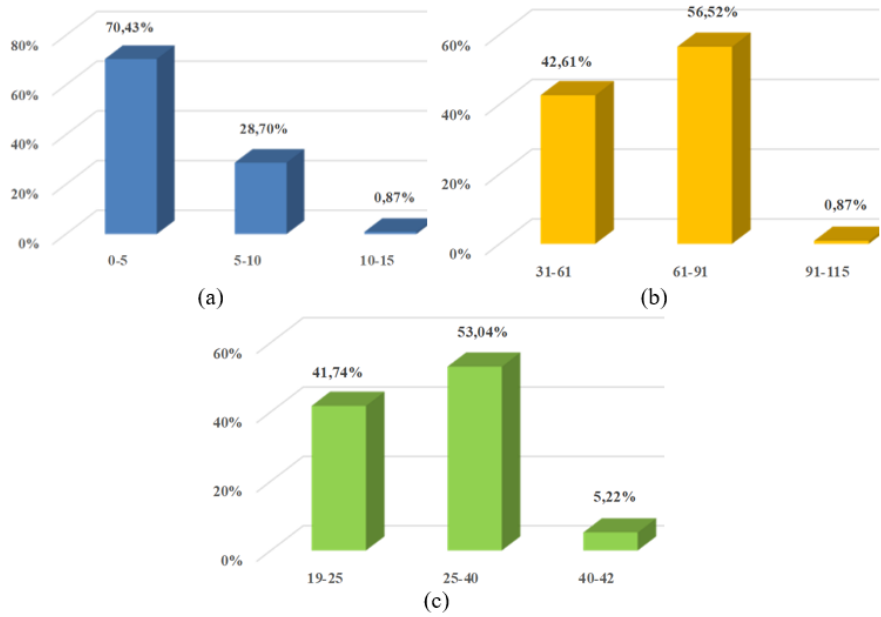

Figure 2. Histograms of The Input Variables in The Raw Database: (A) Lime Content L, (B) Initial Liquid Limit LL_0, And (C) Initial Plastic Limit PL_0.

2.5 Correlation Analysis Between Variables

In addition to the basic descriptive statistics, a correlation analysis was conducted to investigate the relationships between the input and output variables in the literature-based database. The resulting correlation matrix is shown in Figure 3, which reports the linear correlation coefficients for all pairs of variables. The matrix reveals a clear positive correlation between the initial liquid limit (LL_0) and the initial plastic limit (PL_0), which is consistent with their joint role as indicators of the plasticity of the untreated soil.

The plasticity index after treatment (PI) is negatively correlated with lime content L, reflecting the expected reduction in plasticity as lime dosage increases. A weak negative correlation is also observed between the maximum dry unit weight $\gamma_{d\max}$and the optimum moisture content ω_{opt}, in line with the general tendency of Proctor curves for higher dry densities to be associated with lower water contents. Both $\gamma_{d\max}$and ω_{opt}retain some dependence on the initial plasticity indices, although this effect appears less marked than the direct influence of lime content.

While these linear correlations do not capture the full, non-linear nature of the relationships—nor the influence of factors such as mineralogy or curing conditions—they provide useful qualitative insight. In particular, they confirm that the selected inputs carry relevant information for predicting the three target outputs and that there is no excessive redundancy among them, which supports their combined use in a compact ANN model.

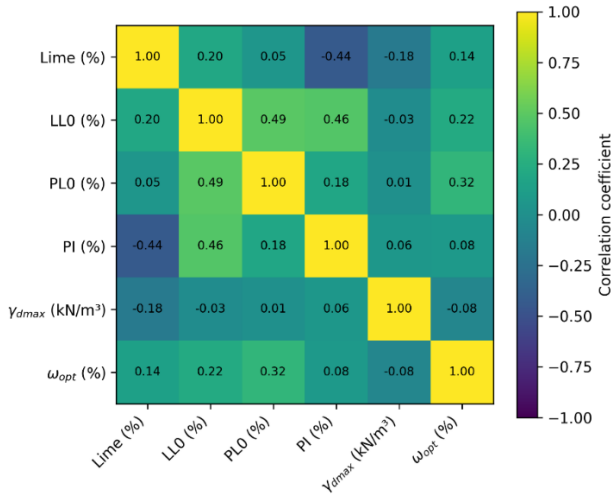

Figure 3. Correlation Matrix of The Input and Output Variables

2.6 Normalization for Subsequent Modelling

In order to place all variables on a comparable numerical scale and to facilitate ANN training, a min–max normalization was applied to each input and output variable:

$$X^* = \frac{X - X_{\min}}{X_{\max} - X_{\min}}$$

where $X_{\min}$and $X_{\max}$denote the minimum and maximum values of the variable in the database. This simple scaling maps all data to the [1, 0] interval and is commonly used in neural network applications.

3. MODELLING FRAMEWORK: GA-OPTIMIZED ANN AND K-FOLD CROSS-VALIDATION

3.1 GA-Based Optimization of The Multi-Output ANN

A multi-output feedforward ANN was developed to map three input variables—lime content, initial liquid limit and initial plastic limit—to three target properties of the stabilized soil: plasticity index, maximum dry unit weight and optimum moisture content. Instead of selecting the network structure by trial and error, a Genetic Algorithm (GA) was employed to search automatically for a suitable architecture. The GA is a population-based optimization procedure inspired by natural selection. At each generation, a population of candidate solutions (here, candidate ANN architectures) is evaluated using a predefined objective function. The fittest individuals are preferentially selected, recombined through crossover and slightly perturbed by mutation, generating a new population that gradually converges towards better solutions. In the present study, each candidate ANN was encoded as a vector of integer hyperparameters specifying the number of hidden layers and the number of neurons in each layer, the activation function assigned to each hidden layer, and the training algorithm used for weight adjustment. For each candidate, the corresponding network was constructed, trained on the normalized literature-based database, and its validation error was used as the fitness (objective) function. The GA was run with a population of 100 individuals over a maximum of 100 generations, using elitism and standard crossover–mutation operators to balance exploration of the architectural space and convergence speed. The evolution of the best and mean fitness values over the generations is illustrated in Figure 4(a)**.** The best fitness curve decreases rapidly during the first generations and then stabilizes at low values, while the mean fitness gradually follows the same trend with higher variability.

This behavior indicates that the GA is able to identify progressively better architectures and to converge towards a region of the search space associated with good predictive performance. The optimization process ultimately led to a compact multi-output ANN with three hidden layers of 8, 7 and 3 neurons, respectively, connecting the 3 inputs to the 3 outputs. The hidden layers employ non-linear activation functions selected by the GA from a predefined set, and network training is carried out using Bayesian regularization in order to enhance generalization. The resulting architecture is depicted schematically in Figure 4(b), which shows the three input nodes, the five neurons of the first hidden layer and the three output nodes corresponding to PI, $\gamma_{d\max}$and ω_{opt}. For this GA-selected configuration, the overall correlation between predicted and observed values on the literature-based database during the optimization stage is approximately $R = 0.94$, indicating a strong global agreement. This architecture, summarized in Table 4.X and illustrated in Figure X, was therefore adopted as the reference multi-output ANN model for the subsequent cross-validation and experimental validation stages.

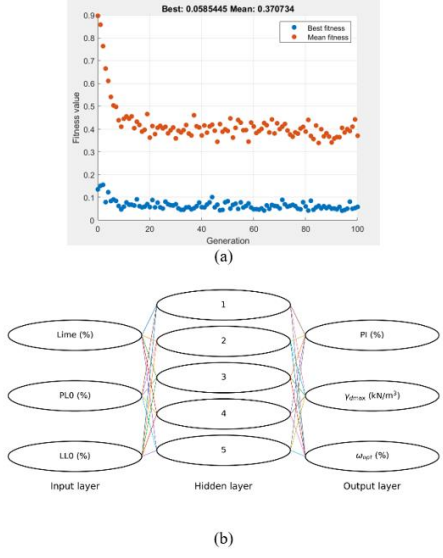

Figure 4. GA-Based Optimization of The ANN Model: (A) Evolution of Best and Mean Fitness Values Over Generations; (B) Schematic Architecture of The Selected Multi-Output ANN.

3.2 K-Fold Cross-Validation Procedure

The generalization capability of the GA-optimized ANN was evaluated using a 5-fold cross-validation procedure. In k-fold cross-validation, the full dataset is partitioned into $k$disjoint subsets (folds). In each run, one-fold is reserved for testing, while the remaining $k-1$folds are used for training; the process is repeated $k$times so that every fold serves once as test data, and the performance metrics are then averaged over the $k$runs. A schematic representation of this procedure for $k=5$is given in Figure 5, where each row corresponds to one run and the hatched block indicates the fold used for validation/testing in that run.

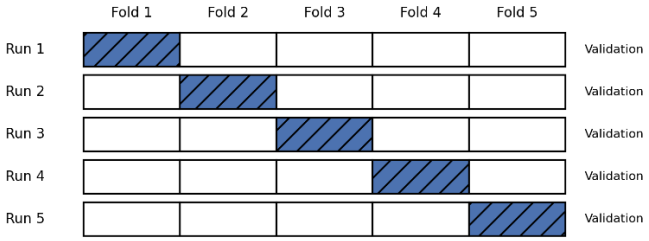

Figure 5. Schematic Representation of 5-Fold Cross-Validation.

In the present work, the normalized literature-based database was divided into five folds of comparable size. For each run, four folds were used to train the GA-selected ANN architecture, with an internal train/validation split handled by the ANN routine to implement early stopping, and the remaining fold was kept as an independent test set. This cycle was repeated until each fold had been used once as test data, thus providing five independent estimates of the prediction performance for each output variable.

The evolution of the mean squared error (MSE) during training is illustrated in Figure 6(a) for a representative run. The curves show the MSE for the training, validation and test subsets as a function of the number of epochs, on a logarithmic scale. The error decreases rapidly during the first epochs and then stabilizes at low values; the best validation performance is obtained after a limited number of epochs (around epoch 19), beyond which additional training does not lead to significant improvement.

The proximity of the training, validation and test curves indicates that overfitting is limited and that the selected architecture exhibits satisfactory generalization behavior. The corresponding regression plot for all data (combining the five test folds) is presented in Figure 6(b). This figure compares the network outputs with the target values and displays both the best-fit regression line and the 1:1 line. The points cluster around the 1:1 line with moderate scatter, and the global correlation coefficient is about $R \approx 0.87$, confirming a good overall agreement between predicted and observed values. The slight deviation of the regression line from the 1:1 line suggests a small systematic bias, but the trend and the ranking of the data are well reproduced.

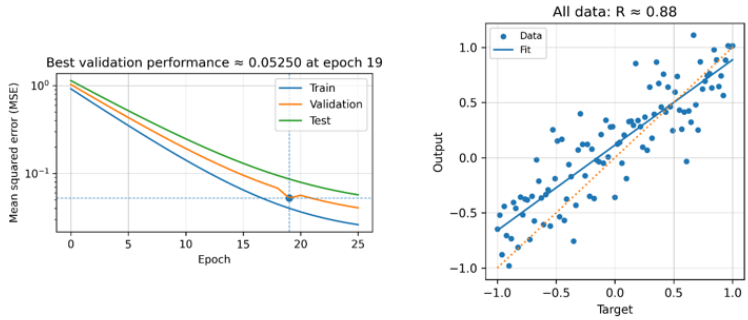

Figure 6. Performance and Regression Results of The GA-Optimized ANN Model.

Despite this decrease in R and the corresponding increase in MSE compared with the GA phase, the cross-validation results show that the model reproduces the main trends of the compiled data with an acceptable level of accuracy. Most predictions remain close to the experimental values, while the larger discrepancies are observed mainly at the edges of the data range or for soil conditions that are sparsely represented in the database. Taken together, Figures 6(a) and 6(b) indicate that the GA-optimized multi-output ANN constitutes a robust and reasonably accurate predictive tool for the plasticity index, maximum dry unit weight and optimum moisture content of lime-stabilized expansive clays within the domain covered by the literature-based database.

4. EXPERIMENTAL PROGRAM

An experimental program was carried out on a natural expansive clay treated with lime in order to provide an independent dataset for validating the GA-optimized ANN model. The soil was sampled from the subgrade of the RN65 road between El-Abadia and Tacheta Zougara (Aïn Defla, Algeria), at a depth of about 1 m, using disturbed samples stored in sealed bags and subsequently tested in the LNHC laboratory in Koléa. The material is a yellowish, highly plastic clay with a natural water content of 22.25%, a bulk dry density of 1.52 t/m³ and a real bulk density of 1.46 t/m³, and was stabilised with a commercial hydrated lime in powder form whose main oxide composition is dominated by CaO (> 83.3%), with minor contents of MgO, Fe_2O_3, Al_2O_3, SiO_2, SO_3, Na_2O, CO_2 and $CaCO_3$, and a white appearance with less than 10% of particles larger than 90 µm.

The influence of lime on soil plasticity was investigated by determining the Atterberg limits of the untreated clay and of soil–lime mixtures with lime contents of 0, 2, 4, 6, 8 and 10% by dry mass. Tests were performed in accordance with NF P 94-051, using the Casagrande cup for the liquid limit and the rolling-thread method for the plastic limit; for each mixture, the liquid limit (LL) and plastic limit (PL) were measured and the plasticity index after treatment was calculated as $PI = LL - PL$, the resulting values forming the experimental targets for the first output of the ANN model. Compaction characteristics of the untreated and lime-treated soils were obtained from standard Proctor tests conducted in accordance with NF P 94-093: for each lime content, a Proctor compaction curve was established by compacting the soil–lime mixture at a series of water contents in a standard Proctor mold, computing the dry unit weight from the compacted mass and mold volume, and identifying, from the dry unit weight versus water content plots, the maximum dry unit weight $\gamma_{d\max}$ and the corresponding optimum moisture content ω_{opt} for each mixture. For the purposes of model validation, a subset of mixtures with lime contents of 0, 6, 8 and 10% by dry mass was retained to build the external validation dataset; for each of these mixtures, the three input variables required by the model (lime content L, initial liquid limit LL_0 and initial plastic limit PL_0 of the untreated soil).

The corresponding target quantities (PI, $\gamma_{d\max}$and ω_{opt}) are available and are used in the next section to confront the predictions of the GA-optimised ANN with independent laboratory measurements under conditions representative of a real engineering project.

4.1 Experimental Behavior of The RN65 Clay Treated with Lime

Atterberg Limits

The Atterberg limits of the RN65 expansive clay were determined for the natural soil and for soil–lime mixtures with lime contents between 0 and 10%. The evolution of liquid limit (LL), plastic limit (PL) and plasticity index (PI) with lime content is shown in Figure 7(a), while Figure 7(b) locates the corresponding points in the Casagrande plasticity chart. The natural soil is a highly plastic silt, with an initial liquid limit of about 60% and a plasticity index of 34%, which places it in the "very plastic silt" field of the Casagrande diagram. As lime is added, LL decreases slightly whereas PL increases markedly, so that PI drops to about 16% at 10% lime. In terms of classification, the soil thus loses more than 50% of its initial plasticity and moves towards the "low-plastic silt" domain in Figure 7(b), illustrating the strong reduction in plasticity induced by lime treatment. These trends are consistent with the classical behavior of montmorillonitic clays treated with lime, where cation exchange and flocculation reduce the thickness of the diffuse double layer, promote aggregation of clay particles and decrease the amount of water required for the liquid state (Holtz, 1969; Dash, 2012; Driss, 2018). The significant increase in PL observed between 0% and 10% lime agrees with the observations of Harichane et al. (2011), who related such changes to the development of a more stable, aggregated structure and the onset of pozzolanic reactions. Similar reductions in PI and improvements in workability for expansive clays and marls stabilized with lime have been reported in Algeria and elsewhere (Benyahia et al., 2020; Sorsa & Agon, 2022; Mohammed et al., 2024). Overall, the Atterberg limit results in Figures 7(a–b) confirm that lime treatment is effective in reducing the plasticity and improving the consistency of the RN65 clay, bringing it into a range more suitable for use as a compacted subgrade or subbase material.

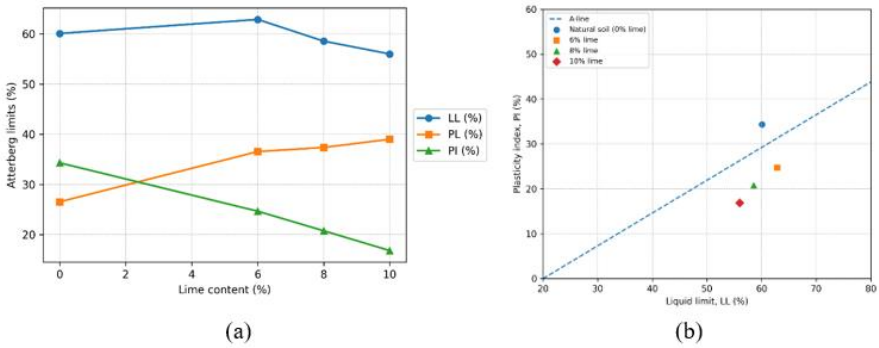

Figure 7. Effect Of Lime on RN65 Clay Plasticity: (A) Atterberg Limits vs. Lime Content; (B) Casagrande Plasticity Chart.

Compaction Parameters

Standard Proctor tests were carried out on the natural RN65 clay and on mixtures with increasing lime contents in order to determine the maximum dry unit weight $\gamma_{d,\max}$ and the optimum moisture content ω_{opt} for each mixture. The corresponding Proctor curves are shown in Figure 8. For the RN65 clay, ω_{opt} increases systematically with lime content, while $\gamma_{d,\max}$ shows an overall decrease from the natural soil to the treated mixtures, with a minimum around 8% lime and a slight increase at 10%.

This behaviour is typical of lime-stabilised clays and suggests that, beyond a lime content close to 8%, additional lime has a limited effect on reducing the dry density and may even lead to a small recovery of $\gamma_{d,\max}$, which can be interpreted as an approach to the critical lime content. This overall shift towards higher ω_{opt} and lower $\gamma_{d,\max}$ may be interpreted in terms of three complementary mechanisms (Harichane et al., 2011).

First, lime induces flocculation and aggregation of clay particles through cation exchange, which transforms the initially dense clay fabric into a course, more open structure and reduces the dry density that can be achieved under a given compaction effort. Second, the specific gravity of hydrated lime is lower than that of the clay minerals, so that substituting part of the soil with lime lowers the maximum dry density of the mixture.

Third, as curing progresses, pozzolanic reactions between lime and the silica and alumina released from clay minerals generate cementitious products that increase the soil's affinity for water and contribute to the higher optimum moisture contents observed in the Proctor tests. The magnitude and direction of the changes in $\gamma_{d,\max}$ and ω_{opt} observed for the RN65 soil are comparable to those reported in experimental studies on expansive clays and marls treated with lime or lime–cement blends (Bell, 1993; Mir, 2018; Benyahia et al., 2020; Sorsa & Agon, 2022; Sambre et al., 2024). In particular, Bell (1993) showed that montmorillonitic soils often exhibit a noticeable drop in dry density and a shift of the Proctor curve towards higher moisture contents as lime content increases up to an optimum or critical value. Taken together, the Atterberg limit and compaction results demonstrate that the RN65 clay behaves in a manner consistent with the broader body of experimental work on lime-stabilized expansive soils and provide a sound experimental basis for the subsequent comparison between the GA–ANN predictions and the measured values of post-treatment PI, $\gamma_{d,\max}$ and ω_{opt}.

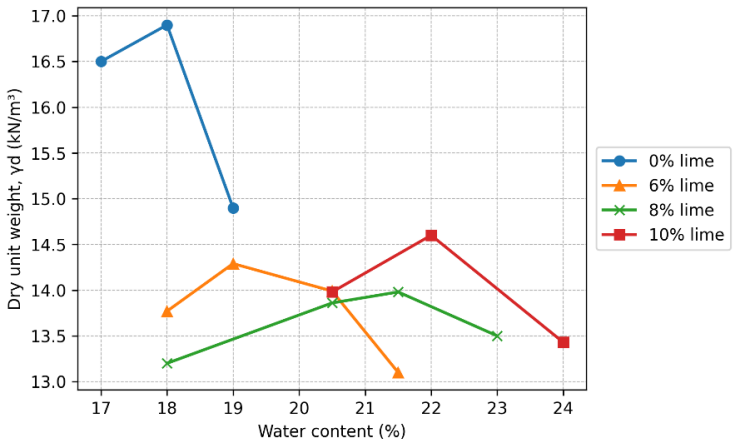

Figure 8. Standard Proctor Curves of The RN65 Clay for Different Lime Contents

Experimental Validation of the GA–ANN Model

The predictive capability of the GA–optimized ANN was evaluated by comparing its outputs with the experimental results obtained for the RN65 expansive clay treated with 0, 6, 8 and 10% lime.

Figure 9(a–c) presents the relationships between experimental and predicted values for the three target variables: post-treatment plasticity index PI, maximum dry unit weight $\gamma_{d\max}$and optimum moisture content ω_{opt}. The prediction accuracy was quantified in terms of relative error, correlation coefficient $R$and coefficient of determination R^2. For each data point, the relative error $RE$was computed as

$$RE(\%) = \left| \frac{Y_{\text{exp}} - Y_{\text{pred}}}{Y_{\text{exp}}} \right| \times 100$$

where $Y_{\text{exp}}$and Y_{pred}denote the experimental and predicted values, respectively.

For the plasticity index, Figure 9(a) shows that the ANN correctly reproduces the marked decrease in $PI$with increasing lime content, which is the key trend from an engineering standpoint. The model predictions exhibit a mean relative error of about 31%, but remain strongly correlated with the experimental values, with $R \approx 0.99$and $R^2 \approx 0.88$. A slight systematic underestimation can be observed, particularly at higher lime dosages, yet the relative ordering of the mixtures is well captured.

The agreement is even better for the compaction parameter $\gamma_{d\max}$, as illustrated in Figure 9(b). The predicted maximum dry unit weights follow the same decreasing pattern as the measured ones and are very close in magnitude for all lime contents. The average relative error is on the order of 8%, and the regression line yields a coefficient of determination of $R^2 \approx 0.96$, indicating an excellent linear correlation between predicted and experimental values.

For the optimum moisture content, Figure 9(c) confirms that the model successfully reproduces the increase in ω_{opt}induced by lime treatment. As for PI, the mean relative error is around 31%, while the correlation remains strong, with $R \approx 0.94$and $R^2 \approx 0.88$. The dispersion around the regression line is moderate and does not alter the overall trend.

Taken together, the results in Figure X(a–c) show that the GA–ANN model provides a realistic representation of the behavior of the RN65 clay treated with lime: it captures both the direction and the magnitude of the changes in PI, $\gamma_{d\max}$and $\omega_{opt}$with acceptable relative errors.

This level of accuracy is sufficient for preliminary design and decision-support applications involving lime-stabilised expansive clays.

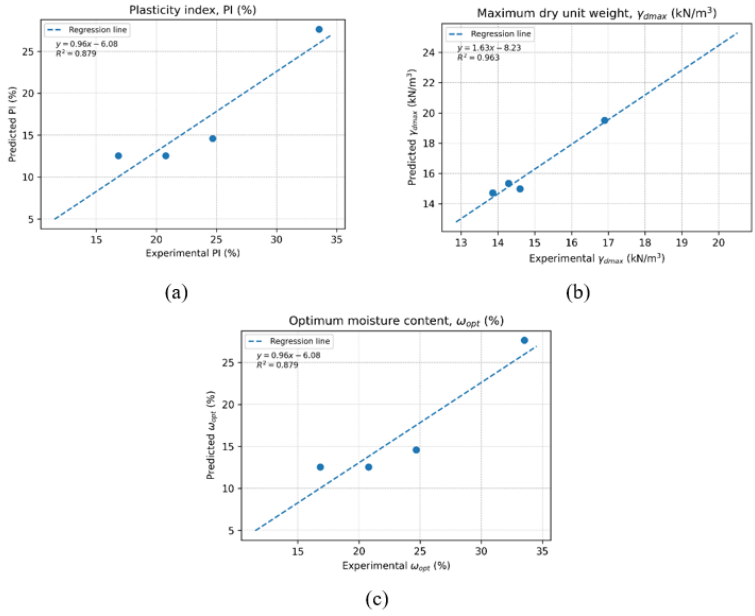

Figure 9. Experimental Vs GA–ANN Predicted PI, $\gamma_{d\max}$And $\omega_{opt}$for The RN65 Clay.

CONCLUSION

This chapter has investigated the prediction of three key properties of lime-stabilized expansive clays—plasticity index after treatment, maximum dry unit weight and optimum moisture content—using a GA-optimized artificial neural network. The model relies only on three simple inputs (lime content and the initial liquid and plastic limits of the untreated soil), which makes it compatible with routine geotechnical investigations and early design stages. A GA–ANN strategy was implemented to automatically select a compact network architecture and its main hyperparameters, and k-fold cross-validation was used to assess internal performance on a literature-based database.

The resulting model showed high correlation coefficients and moderate error levels, indicating that it can reproduce the main relationships between lime content, initial plasticity and the three target properties with satisfactory internal consistency.

External validation on an independent expansive clay from the RN65 road in Algeria confirmed that the GA-optimized ANN can generalize reasonably well beyond the training data. For lime contents of 0, 6, 8 and 10%, the model correctly captured the trends in plasticity index, maximum dry unit weight and optimum moisture content, with acceptable relative errors and strong correlations between measured and predicted values. This level of accuracy is sufficient for preliminary design, screening of lime dosages and sensitivity analyses on the effect of initial plasticity and lime content on compaction specifications.

The approach nonetheless remains empirical and is restricted to the domain covered by the database (fine-grained, medium to highly plastic soils treated with lime in typical road and earthwork ranges), and the external validation set is limited in size. Future work should therefore aim at enlarging the database, incorporating better mineralogical characterization and curing effects, and comparing the GA–ANN framework with other machine learning and hybrid modelling approaches. Despite these limitations, the present study illustrates that combining a curated database with GA-optimized neural networks and cross-validation provides a practical and promising tool to support the design of lime-stabilization schemes in expansive clays.

REFERENCES

Aljanabi, K. R. M., & Salih, N. B. (2023). Using artificial neural networks to predict the unconfined compressive strength of clayey soils stabilized by various stabilization agents. *KSCE Journal of Civil Engineering, 27*(9), 3720–3728. https://doi.org/10.1007/s12205-023-0539-5

Al-Taie, A., Fatahi, B., & Khabbaz, H. (2016). Swell–shrink cycles of lime-stabilised expansive subgrade. *Procedia Engineering, 143*, 1243–1250.

Athanasopoulou, A., & Kollaros, G. (2011). Use of additives to improve the engineering properties of swelling soils in Thrace, Northern Greece. In *Materials Characterisation V* (WIT Transactions on Engineering Sciences, Vol. 72, pp. 327–338).

Bell, F. G. (1993). *Engineering treatment of soils*. London, United Kingdom: E & FN Spon.

Benyahia, S., Boumezbeur, A., Lamouri, B., & Fagel, N. (2020). Swelling properties and lime stabilization of N'Gaous expansive marls, NE Algeria. *Journal of African Earth Sciences, 170*, 103895.

Bozbey, İ., & Garaisayev, S. (2010). Effects of soil pulverization quality on lime stabilization of an expansive clay. *Environmental Earth Sciences, 60*(6), 1137–1151.

Buhler, R. L., & Cerato, A. B. (2007). Stabilization of Oklahoma expansive soils using lime and Class C fly ash. In *Problematic Soils and Rocks and In Situ Characterization* (GSP 162, pp. 1–10). American Society of Civil Engineers.

Choobbasti, A. J., Kutanaei, S. S., Farrokhzad, F., et al. (2010). Influence of cement and lime on the geotechnical properties of a marine clay. *Arabian Journal of Geosciences, 3*, 271–277.

Daniel, J. (2014). Behaviour of lime-stabilised expansive soils. *Unpublished thesis*.

Dayioglu, A. Y., Nasunbul, Y., & Kalkan, E. (2017). Stabilization of expansive Belle Fourche shale clay with different chemical additives. *Applied Clay Science, 146*, 56–69.

Driss, H., Bousshine, B., & Taibi, S. (2021). Effect of lime treatment on the hydro-mechanical behaviour of an expansive clay. *Bulletin of Engineering Geology and the Environment, 80*, 7691–7711.

Estabragh, A. R., Pereshkafti, M. R. S., Parsaei, B., & Javadi, A. A. (2013). Stabilised expansive soil behaviour during wetting and drying. *International Journal of Pavement Engineering, 14*(4), 418–427. https://doi.org/10.1080/10298436.2012.746688

Farghaly, A. A., El-Shater, A., Abdel Naiem, M. A., & Hamdy, F. (2020). Lime addition chemical stabilization of expansive soil at Al-Kawamil city, Sohag region, Egypt. *Advances in Computational Design, 5*(1), 1–11. https://doi.org/10.12989/acd.2020.5.1.001

Gadouri, H., Harichane, K., & Ghrici, M. (2017). Effect of calcium sulphate on the geotechnical properties of stabilized clayey soils. *Periodica Polytechnica Civil Engineering, 61*(2), 256–271. https://doi.org/10.3311/PPci.9359

Ghobadi, M. H., Abdilor, Y., & Babazadeh, R. (2014). Stabilization of clay soils using lime and effect of pH variations on shear strength parameters. *Bulletin of Engineering Geology and the Environment, 73*(3), 611–619. https://doi.org/10.1007/s10064-013-0563-7

Harichane, K., Ghrici, M., & Kenai, S. (2017). Effect of lime and natural pozzolana on the swelling and compressibility characteristics of expansive clays. *Geotechnical and Geological Engineering, 35*, 1717–1730.

Harichane, K., Ghrici, M., Kenai, S., & Grine, K. (2011). Use of natural pozzolana and lime for stabilization of cohesive soils. *Geotechnical and Geological Engineering, 29*(5), 759–769. https://doi.org/10.1007/s10706-011-9415-z

Harish, G. R. (2017). Studies on stabilization of black cotton soil using lime. *International Research Journal of Engineering and Technology, 4*(6), 1725–1727.

Ismaiel, H. A. H. (2006). Treatment and improvement of the geotechnical properties of an Egyptian expansive clay. *Alexandria Engineering Journal, 45*(2), 271–284.

Jeremiah, J. J., Abbey, S. J., Booth, C. A., & Kashyap, A. (2021). Results of application of artificial neural networks in predicting geo-mechanical properties of stabilised clays—A review. *Geotechnics, 1*(1), 147–171. https://doi.org/10.3390/geotechnics1010008

Jha, A. K., & Sivapullaiah, P. V. (2015). Role of fly ash and lime in the improvement of swelling behaviour of an expansive soil. *Soils and Foundations, 55*(3), 525–534.

Kechouan, B., & Nechnech, A. (2015). Influence de la chaux sur le comportement de marls expansifs d'Algérie. *Journal of Materials and Engineering Structures, 2*(2), 91–104.

López-Lara, T., Hernández-Zaragoza, J. B., Horta-Rangel, J., Rojas-González, E., López-Ayala, S., & Castaño, V. M. (2017). Expansion reduction of clayey soils through surcharge application and lime treatment. *Case Studies in Construction Materials, 6*, 109–119. https://doi.org/10.1016/j.cscm.2017.06.003

Luo, Z., Zhang, J., Huang, Y., & al. (2025). Data-driven prediction of unconfined compressive strength in stabilized soils using machine learning. *SN Applied Sciences, 7*, 7669. https://doi.org/10.1007/s42452-025-07766-9

Marcon, A. F., Corrêa, J. F., & Trichês, G. (2015). Improvement in physical and mechanical properties of soils by the addition of lime for paving roads. *Transportation Research Record: Journal of the Transportation Research Board, 2473*(1), 209–214.

Mir, B. A. (2015). Some studies on the effect of fly ash and lime on physical and mechanical properties of expansive clay. *International Journal of Civil Engineering, 13*(3B), 203–212. https://doi.org/10.22068/IJCE.13.3.203

Muhmed, A., Mohamed, M. H. A., & Khan, A. (2024). Prediction of unconfined compressive strength of lime treated soils. *Geomechanics and Geoengineering*. Advance online publication. https://doi.org/10.1080/17486025.2024.2319612

Najafian Jazi, F., Mir Mohammad Hosseini, S. M., Ghasemi-Fare, O., & Rockaway, T. D. (2024). Experimental evaluation of stress history effect on compressibility characteristics of lime-stabilized expansive soils. *Geomechanics and Geoengineering, 20*, 21–34.

Onyelowe, K. C., Moghal, A. A. B., Ebid, A., Rehman, A. U., Hanandeh, S., & Priyan, V. (2024). Estimating the strength of soil stabilized with cement and lime at optimal compaction using ensemble-based multiple machine

learning. *Scientific Reports, 14*, 15308. https://doi.org/10.1038/s41598-024-66295-4

Ozioko, H. O., & Eze, E. E. (2025). Predictive modeling of CBR and compressibility in lime stabilized lateritic soil using machine learning and Pchip data augmentation. *Discover Civil Engineering, 2*, 141. https://doi.org/10.1007/s44290-025-00304-x

Ramlakhan, B., Kumar, S. A., & Arora, T. R. (2013). Effect of lime and fly ash on engineering properties of black cotton soil. *International Journal of Emerging Technology and Advanced Engineering, 3*(11), 535–541.

Sambre, T., Endait, M., & Patil, S. (2024). Sustainable soil stabilization of expansive soil subgrades through lime–fly ash admixture. *Discover Civil Engineering, 1*, 65. https://doi.org/10.1007/s44290-024-00063-1

Shah, A., Thaker, T., Shukla, V., & Ranpura, P. (2024). Efficient predictive modeling of resilient modulus in stabilized clayey soil using automated machine learning. *Construction and Building Materials, 454*, 137678. https://doi.org/10.1016/j.conbuildmat.2024.137678

Sorsa, A., & Agon, E. (2022). Lime stabilization of expansive clay soil of Jimma town, Ethiopia. *Civil Engineering Infrastructures Journal, 55*(2), 211–222.

Tabarsa, A., Amini, A., & Karimi, M. (2021). Unconfined compressive strength prediction of soils stabilized using artificial neural networks and support vector machines. *Frontiers of Structural and Civil Engineering, 15*(4), 905–923. https://doi.org/10.1007/s11709-021-0689-9

Wang, J., Chen, G., Chen, Y., Ye, Z., Lin, M., Su, R., & Hu, N. (2024). Intelligent mixture optimization for stabilized soil containing solid waste based on machine learning and evolutionary algorithms. *Construction and Building Materials, 445*, 137794. https://doi.org/10.1016/j.conbuildmat.2024.137794

Zhang, J.-R., & Cao, X. (2002). Stabilization of expansive soil by lime and fly ash. *Journal of Wuhan University of Technology – Materials Science Edition, 17*, 73–77.

ISBN: 978-625-93333-4-2